Multiomic Profiling Reveals Metabolic Alterations Mediating Aberrant Platelet Activity and Inflammation in Myeloproliferative Neoplasms

Fan He[1], Angelo B.A. Laranjeira[1], Tim Kong[1], Alice Liu[2], Katrina Bark[2], Nina M. Lasky[2], Daniel A.C. Fisher[1], Maggie J. Cox[1], Mary Fulbright[1], Layow Yu[1], Stephen M. Sykes[2], Angelo D'Alessandro[3], Jorge Di Paola*[2], Stephen T. Oh*[1]

[1]Division of Hematology, Department of Medicine, School of Medicine, Washington University School of Medicine, St. Louis, MO, USA

[2]Division of Hematology & Oncology, Department of Pediatrics, School of Medicine, Washington University School of Medicine, St. Louis, MO, USA

[3]Department of Biochemistry and Molecular Genetics, University of Colorado-Anschutz Medical Campus, Aurora, CO, USA

*Co-corresponding authors.

ABSTRACT

Prior studies by our group and others have demonstrated that platelets from patients with myeloproliferative neoplasms (MPNs) exhibit a hyperreactive phenotype. However, a complete understanding of platelet alterations in MPNs remains lacking, and the mechanisms by which platelets contribute to MPN-related thrombosis, as well as other MPN disease features, are incompletely understood. In this study, utilizing multiomic approaches to interrogate platelet phenotypes in patient samples, in conjunction with relevant MPN animal models, we aim to investigate mechanisms of dysregulated platelet activity in MPNs, and explore how these findings may be leveraged to uncover novel therapeutic strategies.

We initially studied platelet activation in peripheral blood from patients with essential thromobocythemia (ET) and compared to age-, sex-matched healthy controls. We found significantly increased P-selectin exposure in conjunction with increased platelet-leukocyte aggregates indicating activation of platelets from ET patients. To investigate the transcriptional signature of PBMCs and platelets at the single cell level, we performed single cell RNA-seq (scRNA-seq) in PBMCs from ET patients and healthy controls. Monocytes were increased in ET patients and displayed the highest inflammation index, implicating monocytes as the primary source of inflammation in ET. Aside from the quantitative increases of platelets in ET patients, we demonstrated strong enrichment of platelet activation, mTOR and oxidative phosphorylation (OXPHOS) genes in platelets from ET patients. Proteomic data confirmed the activation of OXPHOS and mTOR pathways in platelets from MPN patients. Metabolomics analysis revealed distinct metabolic phenotypes consisting of elevated tricarboxylic acid (TCA) cycle components, ATP generation and lower alpha-ketoglutarate (α-KG), in platelets from MPN patients, all consistent with enhanced OXPHOS and mTOR activities. Enhanced mitochondrial respiration at both baseline and after *ex vivo* stimulation with the platelet agonist thrombin receptor activator peptide (TRAP6) by extracellular flux analysis confirmed the bioenergetic alterations in platelets from MPN patients.

α-KG is a key TCA cycle intermediate, which inhibits PI3K/AKT/mTOR pathway signaling via suppression of ATP synthase. α-KG supplementation drastically reduced oxygen consumption

and ATP generation in platelets from MPN patients. We further investigated the effects of α-KG on MPN platelet activation. *Ex vivo* incubation of platelets from both MPN patients and *Jak2* V617F knock-in mice with α-KG significantly reduced platelet surface P-selectin and integrin $\alpha_{2b}\beta_3$ activation. Additionally, α-KG inhibited the spreading and adhesion of platelets from *Jak2* V617F knock-in mice to fibrinogen-coated surfaces. Platelet phosphoblots demonstrated significant downregulation of p-AKT and p-ERK after treatment with α-KG, suggesting the involvement of PI3K/AKT/mTOR and MAPK pathways in the inhibitory effects of α-KG on platelet activation. Thus, α-KG inhibited platelet hyperreactivities in both human and mouse MPN samples.

To test the therapeutic impact of α-KG on MPN disease features, we treated *Jak2* V617F knock-in mice with α-KG for 6 weeks. Oral α-KG supplementation decreased splenomegaly and reduced elevated platelets and hematocrit. Additionally, monocytes were significantly decreased as early as 2 weeks after α-KG treatment in *Jak2* V617F knock-in mice. Consistently, RNA-seq of bone marrow samples from α-KG treated mice revealed inhibition of heme metabolism, OXPHOS and mTOR signaling pathways. In *ex vivo* studies with MPN patient CD34+ cells, α-KG treatment for 10 days led to a decrease in CD41+ CD61+ cells, suggesting decreased megakaryocyte commitment. We further observed that α-KG incubation significantly decreased the secretion of proinflammatory cytokines from sorted CD14+ human monocytes. Mass cytometry analysis of whole blood from MPN patients demonstrated inhibition of MAPK pathway signaling after α-KG treatment. Taken together, these results suggest that α-KG supplementation may exert therapeutic effects through both direct inhibition of MPN platelet activity and via quenching of monocyte hyper-inflammation.

In summary, these studies reveal a previously unrecognized metabolic disorder in platelets from MPN patients and highlight a prominent role for α-KG and mTOR signalling in aberrant MPN platelet activity and monocyte-driven inflammation. These findings have potential relevance for novel therapeutic approaches for MPN patients.

INTRODUCTION

Philadelphia-negative chronic myeloproliferative neoplasms (MPNs), including polycythemia vera (PV), essential thrombocythemia (ET), and primary myelofibrosis (PMF), are clonal hematopoietic disorders characterized by overproduction of mature blood cells such as erythrocytes, granulocytes, and/or platelets[1]. MPN patients face significantly elevated risks of thrombosis; the pooled prevalence of overall thrombosis among patients with MPN reached 20% at diagnosis[2]. Cytoreductive therapies and aspirin are commonly used for the treatment of MPN patients to reduce thrombosis risk[3].

Thrombosis is a multifactorial event involving complex interplays among blood cells, endothelial cells, coagulation cascade and inflammatory mediators; increased blood cell counts, Jak2 mutation burden, and chronic inflammation status all contribute to prothrombotic phenotypes observed in MPN patients[4]. Increased thrombin generation, elevated levels of procoagulant microparticles and soluable p-selectin in serum suggested the hyperreactivity of platelets in MPN patients[5-7]. Interestingly, platelets from homozygous *JAK2* V617F knock-in mice simulating PV have reduced aggregation and increased bleeding time whereas heterozygous *JAK2* V617F mice with ET phenotype showed increase in platelet aggregation and reduced bleeding time[8,9]. Chronic inflammation is a hallmark of MPNs regardless of subtypes[10]. Aside from its classical functions in

hemostasis, platelets also contribute to thromboinflammatory processes by directly interacting with leukocytes[11]. Elevated platelet-leukocyte aggregates has recently been found to be an independent risk factor for thrombosis occurrence in MPN; it suggested that platelets may be a mediator between thrombosis and inflammation[12-14]. However, current evaluation of risk of MPN-associated thrombosis only consider quantitative change in platelets, the qualitative differences of platelets in MPNs have not been systematically evaluated.

Despite being anucleate, platelets contain mitochondria. Mitochondria supplies around 40% energy during resting state, and the rates of OXPHOS boost during active state, such as platelet activation and secretion, to meet the increased demand of energy[15]. The dysregulation of platelet metabolism has been reported in diverse diseases, such as diabetes mellitus, sepsis and pulmonary hypertension[15]. Previously, we reported TNF-α-induced mitochondrial reprogramming may mediate platelet hyperreactivity during aging[16]. However, it remains poorly understood if metabolism dysregulation exists in platelets from MPN patients.

Here, we applied multiomic approaches in conjunction with functional interrogation of platelets from MPN patients. Our results demonstrated platelet hyperreactivity in MPN patients. We also identified metabolic alterations, such as oxidative phosphorylation, and mTOR signaling activation that might contribute to platelet hyperreactivity. In addition, we demonstrated that α-KG supplementation inhibits platelet activation and megakaryopoiesis, at least in part due to inhibition of cellular metabolism and mTOR pathway signaling, identifying a promising therapeutic strategy for MPN patients.

RESULTS

Platelets from ET patients show significantly increased p-selectin level and platelet-leukocyte aggregates (PLA) formation

First, platelet activation was measured in peripheral blood from 25 MPN (ET = 17, MF = 8) patients and healthy individuals (HI, n = 7, Table 1). There was no significant differences of age and sex between ET patients and healthy controls. Platelets from ET and MF patients had significantly higher basal P-selectin, a marker of α-granules activation and secretion, compared to healthy controls, with no significant differences observed after platelet agonist thrombin receptor activator peptide (TRAP6) stimulation (Figure 1A & 1B). We also observed higher percentage of PLA formation in peripheral blood from ET patients (Figure 1C & 1D), which is consistent with previous reports[17]. Platelets from ET patients had higher αIIbβ3 integrin activation following TRAP6 stimulation but there was no difference at baseline (Figure 1E). P-selectin exposure positively correlated with αIIbβ3 integrin activation and PLA formation as expected (Figure 1F, 1G & 1H & Table 2). Platelets from patients carrying the *JAK2* mutation exhibited stronger responses to TRAP6 stimulation than those with *CALR* mutations with higher P-selectin exposure and αIIbβ3 integrin activation; reduced platelet activation is consistent with a lower risk of thrombosis in patients carrying the *CALR* mutation than *JAK2*-mutated patients reported before (Figure S1A & Table 3)[18]. Platelet aggregometry showed decreased platelet responses in MPN patients when compared to HI, likely related to the effects of aspirin (Figure S1B & S1C). However, platelet responses were significantly higher in patients with the *JAK2* mutation when compared to those carrying *CALR* mutations (Figure S1D). Thus, elevated p-selectin levels, increased αIIbβ3 integrin activation and PLA formation indicate hypereactivity of platelets in patients with MPNs.

Platelets from ET patients show upregulation of platelet activation and oxidative phosphorylation pathway genes

Based on our findings of increased platelet reactivity and PLA, and to better understand the transcriptional landscape of platelets and other blood cells from MPN patients, we performed single-cell RNA-Seq (scRNA-seq) of PBMCs from ET patients (n = 5) and age- and sex-matched HIs (n = 3) (Figure 2A & Table 4). Cell types were assigned with canonical transcripts, such as *CD14* for CD14+ monocytes, *CD8A* for CD8+ T cells and *PPBP* for platelets (Figure 2B & S2A). Cell clusters showed distinct transcriptional enrichments in the dot plot (Figure S2B). Subsquent cell composition analysis showed that CD4 T cells were the most abundant cell type in both ET and HI, accounting for 30%–55% of cells (Figure S2C). The percentage of platelets significantly increased in ET patients with a trend of higher monocytes (Figure S2C). Platelets were further clustered into 10 distinctive groups using unsupervised clustering method (Figure 2C & 2D). Platelets in cluster 6 exhibited the highest score for the platelet activation gene set index and they were all from ET patients, whereas cluster 0 showed the lowest score and it is mostly represented by platelets from HI (Figure 2C & 2E). We then interrogated the overlap of the platelet activation gene set (composed of 261 genes) with differentially expressed genes in platelets from HI and ET. While none of the 261 genes were enriched in platelets from HI, 62 genes were upregulated in platelets from ET, including *SELP*, *PF4* and *GP1BA*, (Figure 2F & 2G). Consistently, unbiased GO and KEGG analysis showed the enrichment of genes involved in platelet activation in platelets from ET patients (Figure S2D-S2F). Gene score enrichment analysis (GSEA) analysis confirmed the transcriptional activation of platelet activation and IFN-γ pathways, and showed upregulation of genes involved in PI3K_AKT_mTOR signaling and oxidative phosphorylation (OXPHOS) in the platelets from ET patients (Figure S2G-S2J). To validate our a scRNA-seq findings, we analyzed GSE2006, a publically available comparative microarray dataset from ET platelets and healthy controls, and found enrichment of platelet activation and OXPHOS gene sets in platelets from ET patients (Figure S3). Thus, these results not only support the activation of platelets in MPN patients, but also led to the hypothesis that platelet metabolic alterations contributes to the platelet hyperreactivity observed in MPNs.

Gene expression analyses of IFN-γ and inflammation response pathways revealed that monocytes have the highest score of all blood cells analyzed (Figure S4A & S4B). Further clustering showed that 2 distinctive monocyte clusters (8 and 9) are the ones exhibiting highest transcriptional levels of IFN-γ pathway genes (Figure S4C). Interestingly, these two clusters showed robust enrichments of monocytes from ET patients and higher levels of *PPBP*, a platelet marker, which suggest a role of platelets in activating monocytes (Figure S4D).

Metabolomics and proteomics analysis revealed elevated mitochondrial activities in platelets from MPN patients

To better understand the metabolic alterations of platelets from MPN patients, we performed ultra-high-performance liquid chromatography coupled with mass spectrometry (LC-MS) metabolomics on plasma and washed platelets from MPN patients along with age- and sex-matched HIs (Figure 3A & Table 5, ET = 12, PV = 7, MF = 9, HI = 8). Multivariate analysis was conducted to reduce dimensionality for visualization and there was a clear distinction between clusters of platelets from HI and MPN on the axis of principal component 1 (Figure 3B). Differentially accumulated

metabolites (DAMs) were defined as those exhibiting a log fold change > 0.5 and $p < 0.05$ between MPN and HI. For MPN vs. HI, 24 of 181 (13.3%) were upregulated and 19 of 181 (10.5%) were downregulated; 6-Phosphogluconate, alpha-ketoglutarate (α-KG), succinate, and ATP were among top DAMs (Figure 3C & S5A). In contrast, the lack of differences in plasma metabolites from the same individuals suggested that the metabolic alterations in platelets are intrinsic modifications instead of changes in microenvironment (Figure S5B & S5C). Lower glucose in conjuction with higher pyruvate levels indicates the activation of glycolytic pathways in platelets from MPN compared to HI (Figure 3D). Increased Krebs cycle components succinate and malate, paralleled with higher ATP levels, suggested elevated mitochondrial activities in platelets from MPN compared to HI (Figure 3D). Platelet proteomics also showed evident separation of MPN from HI in PCA plots, and elevated mitochondrial OXPHOS complex components in platelets from MPN (Figure 3E & 3F). The enrichment of mTORC1 pathway in platelets from MPN patients paralleled our scRNA-seq and metabolomics results (Figure 3G) since it have been found to drive mitochondrial biogenesis and OXPHOS activities[19]. Measurement of mitochondrial protein and OXPHOS complexes by western blot demonstrated significant increases of TOM-20, a mitochondrial marker, and complex V protein, the ATP synthase responsible for energy generation, in platelets from ET patients (Figure 3H). Thus, these results provide evidences for elevated mitochondrial activities and mTOR signaling activation in platelets from MPN compared to HI.

Platelets from MPN patients displayed bioenergetic alterations, which can be reverted by α-KG supplementation

To interrogate the bioenergetic alterations in platelets from MPN patients, platelets were isolated for Seahorse extracellular flux analysis. Platelets from MPN patients showed increased rates of basal respiration and ATP generation after correction for non-mitochondrial oxygen consumption rate (OCR); which suggested elevated physiological mitochondrial respiration (Figure 4A & 4B). Similar changes were observed in platelets from *Jak2 V617F* mice (Figure S6A). The reserve capacity, calculated as the difference between maximal and basal OCR, is also significantly greater in platelets from MPN patients (Figure 4B). Notably, the *ex vivo* stimulation of platelets from MPN with TRAP6 showed greater OCR responses than in platelets from HI, indicating a larger reserve capacity when energy demand is increased (Figure 4C). A positive correlation was found between basal respiration and P-selectin exposure on platelets (Figure S6B). Altogether, our results demonstrated elevated mitochondrial respiration and coupling ATP generation in platelets from MPN patients.

α-KG is a key intermediate of TCA cycle, which is produced from isocitrate by oxidative decarboxylation or from glutamate by oxidative deamination[20]. Recent studies found that α-KG supplementation inhibits ATP generation via the direct suppression of ATP synthase and plays a critical role in alleviating aging and inflammation[21,22]. A recent report showed that α-KG inhibits thrombosis and inflammation by via inactivation of Akt phosphorylation[23]. Based on the activation of OXPHOS and mTOR signaling along with the decreases of α-KG in platelets from MPN patients, we tested whether α-KG supplement could revert the metabolic alterations of platelets in the context of MPN. The incubation of platelets in the presence of Octyl-α-KG significantly reduced basal respiration, ATP generation and reserved capacity in platelets from both MPN and HI (Figure 4D-4F). α-KG inhibits proton pump in ATP synthase as expected, which is reflected by increased proton leak as well as increased extracellular acidification rate (ECAR) (Figure 4D &

4F). Thus, α-KG supplement modified the metabolic phenotype of platelets from MPN patients by inhibiting mitochondrial activities. A similar inhibition of mitochondrial respiration by α-KG was observed in UKE-1, an ET transformed acute leukemia cell line (Figure S6C).

α-KG inhibited platelet activation through the suppression of ATP synthase

After demonstrating α-KG's inhibition of platelet metabolism, we further evaluated the influence of α-KG on platelet activities. *Ex vivo* incubation of Octyl-α-KG significantly reduced the expression of P-selectin and αIIbβ3 integrin activation following TRAP6 treatment on washed platelets from MPN patients (Figure 5A). A similar inhibitory effect of α-KG was observed in platelets from *Jak2 V617F* mice (Figure S7A). Since αIIbβ3 downstream signaling (outside in signaling) plays a critical role in platelet spreading and aggregation, we performed static platelet spreading and adhesion assays on platelets from *Jak2 V617F* mice. The *ex vivo* incubation with α-KG significantly decreased the number and area of platelet adhesion to a fibrinogen-coated surface; α-KG also inhibited platelet spreading induced by PAR-4 agonist peptide (Figure 5B). Consistently, α-KG induced a dose-dependent inhibition of platelet aggregation (Figure 5C). Importantly, 2% α-KG supplement in drinking water inhibited P-selectin exposure and αIIbβ3 integrin activation on platelets in both wt and *Jak2 V617F* knock-in mice following thrombin stimulation (Figure 5D). Mechanistically, previous reports have shown that phosphorylation of Stat3, Akt and Erk play essential roles in platelet activation. α-KG inhibited p-Stat3, p-Akt and p-Erk1/2 of platelets from MPN patients without affecting the total amount of these proteins following TRAP6 stimulation in a dose-dependent manner (Figure 5E). Moreover, α-KG downregulated p-Stat3, p-Akt and p-Erk1/2 when platelets were activated with different agonists, including TRAP6, collagen and ADP (Figure 5F). Oligomycin, a widely used inhibitor of the ATP synthase, showed similar downregulation of p-Akt and p-Stat3, suggesting a role for ATP synthase in platelet activation (Figure 5G)[24]. Finally, the addition of α-KG increased mitochondrial membrane potential significantly as it inhibited the proton pump of complex V while decreased intracellular ATP level in both MEG-01 and UKE-1 cell lines (Figure S7B-S7D). Collectively, our data demonstrated that α-KG supplementation inhibits platelet activation in MPN, which is at least partially due to the suppression of the ATP synthase.

α-KG exerts therapeutic impacts on MPN and inhibits megakaryopoiesis *in vivo*

After demonstrating the effects of α-KG on reducing platelet hyperreactivity *ex vivo*, we next sought to investigate the therapeutic impact of α-KG in MPNs *in vivo*. Mice engrafted with *Jak2 V617F* bone marrow were supplemented with 1% α-KG in drinking water or regular water as control for 6 weeks (Figure 6A). As expected, *Jak2 V617F* bone marrow transplantation led to the development of MPN, including splenomegaly, increased WBC, RBC and platelet count (Figure 6B & 6C). α-KG supplement markedly reduced splenomegaly, platelet count and RBC without affecting body weight and lymphocyte count (Figure 6B, 6C & S8A). A trend of decreased MPP2 cells in bone marrow from α-KG-supplemented mice supported the suppression of megakaryopoiesis and erythropoiesis (Figure S8B). HE staining of bone marrow confirmed the decreases of megakaryocytes in α-KG supplemented mice (Figure S8D). Importantly, α-KG supplementation to wild type mice does not affect WBC and myeloid differentiation (Figure S8E). To further characterized the effects of α-KG on megakaryopoiesis, sorted human CD34+ cells

were differentiated into megakaryocytes *in vitro* with the addition of cytokines (Figure 6D). The decrease of CD41- and CD61-dual positive megakaryocytes in the presence of α-KG supported the observation of lower platelet counts in α-KG supplemented-mice (Figure 6E). Moreover, α-KG inhibited megakaryocytic maturation of MEG-01 cells *in vitro* (Figure S8J). Interestingly, α-KG treatment also reduced LSK cells in mice, suggesting a role of α-KG in hematopoietic stem cells regulation (Figure 6F). Consistently, α-KG led to the reduction of myeloid colonies in both wt and *Jak2 V617F* c-KIT+ hematopoietic stem and progenitor cells, but to a larger degree in *Jak2 V617F* cells (Figure 6G). Bulk RNA sequencing of bone marrow from control and 1% α-KG-supplemented mice cluster separately in the PCA plots (Figure S8F). GSEA analysis showed inhibtion of OXPHOS, mTORC1 and myeloid differentiation pathways in α-KG group (Figure S8G & S8H). Expression levels of *Gata1* and *Epor*, critical mediators of platelet and RBC differentiation, decreased in α-KG-supplemented mice (Figure S8I). Downregulation of *Cdk1* and *Cdkn3* in α-KG-supplemented mice suggested cell cycle arrest (Figure S8I). Thus, α-KG suppresses MPN progression and megakarypoiesis in *Jak2 V617F* transplant mice.

α-KG inhibited monocytes activation and hyperinflammation

While MPN is caused by genetic mutations in HSC, its progression is driven, at least in part, by inflammation[10]. Various pro-inflammatory cytokines were found elevated in MPN patients' serum and they often correlated to prognosis[25]. Previously, our group showed that monocytes play a critical role in hyperinflammation that characterizes MPNs[26,27]. Since monocyte counts decreased as early as two weeks in the α-KG-supplemented mice (Figure S8C), we sought to investigate if α-KG affects monocyte activation and inflammation. We first examined cytokines in serum from MPN patients and found significant elevation of pro-inflammatory cytokines, including TNF, IFN-γ, IP-10 and IL-6, in ET patients when compared to HI (Figure 7A & Table 6). The *ex vivo* incubation of α-KG with sorted CD14+ human monocytes significantly decreased the secretion of pro-inflammatory cytokines (Figure 7B). Bulk RNA-seq results demonstrated that monocytes incubated with α-KG showed downregulation of genes in involved interferon pathways and inflammation response (Figure 7C & 7D). Mass cytometry analysis of whole blood from MPN patients demonstrated inhibition of MAPK pathway signaling in monocytes following α-KG treatment (Figure 7E). Thus, α-KG inhibited monocyte activation and inflammation, which might also contribute to its therapeutic effects on MPN.

DISCUSSION

Thrombosis and bleeding complications are common in MPN, calling for a better understanding of platelet biology. Some reports suggest hyperreactivity and enhanced secretion of platelets in MPN, but lack in-depth analysis[14,17,28-32]. In this study, we, for the first time, demonstrated the hyperreactivity and underlying enhanced metabolic activities and mTOR signaling pathway in platelets from MPN patients. Our scRNA-seq not only showed robust activation of platelet activation genes in platelets from ET patients, but also revealed the heterogeneity of it. Consistant with elevated secretion of proinflammatory cytokines reported before, monocytes were identified as the major mediator of inflammation and IFN-γ activation in MPN blood cells[10,26,27]. Furthermore, the correlation of elevated transcription of IFN-γ genes with PPBP suggested the involvement of platelets aggregates in monocytes activation considering the increased PLA formations in MPN.

A recent large-scale gene expression profiling of platelets from MPN patients suggested the activation of OXPHOS and mTORC1 signaling pathways in all three subtypes of MPNs[33]. Importantly, these differentially expressed genes robustly predict MPN progression, highlighting the importance of platelet biology in MPNs[33]. Our proteomics data validated the activation of OXPHOS and mTORC1 proteins in platelet from MPN. Metabolomics analysis identified metabolic abnormalities of enhanced TCA cycle and lower α-KG level in platelets from MPN patients. Furthermore, our results demonstrated that α-KG supplement inhibits platelet hyperreactivity and MPN development through suppression of ATP production and PI3K/AKT/mTOR pathway, providing a proof of concept for targeting α-KG and mTOR in MPNs.

Metabolic alterations in MPNs have been reported before. Glutaminase inhibitor suppresses the growth of *JAK2* V617F mutant cell lines and CD34+ cells from MPN patients[34]. IDH2 inhibitor showed efficacy in cells from MPN patients carrying both JAK2 and IDH2 mutations[35]. Recently, elevated glycolysis is found in JAK2-mutant hematopoietic cells from MPN mouse models and it can be targeted to treat MPNs[36]. Our metabolomics results also revealed enhanced glycolysis in platelets from MPN patients. Of note, concurrent mTOR signaling activation and enhanced mitochondrial activities in platelets from MPN patients highlight the significance of metabolic alterations in platelet hyperreactivation and MPN pathogenesis. The correlation of basal OCR with p-selectin exposure and greater OCR responses in response to TRAP6 stimulation bridges metabolic abnormalities with platelet hyperreactivity. Furthermore, we demonstrated that α-KG suppresses platelet hyperreactivity in MPN patient samples and MPN mouse models.

α-KG is also important for the enzymatic function of many α-ketoglutarate-dependent proteins, including jumonji domain-containing histone demethylases, tets proteins mediating DNA methylation and Prolyl-hydroxylase domain enzymes degrading the HIF proteins[20]. α-KG has been reported to maintain embryonic stem cell pluripotency via epigenetic regulations, but its effects on hematopoiesis remained unknown[37]. We demonstrated the inhibition of myeloid differentiation in *Jak2* V617F transplant mice but not in wild type mice, highlighting the effectiveness and safety of α-KG in treating MPNs. Our data aslo validated a role for mTOR signaling inhibition by α-KG, more research are needed to explore the mechanistic targets of α-KG in human hematopoietic stem cells.

Some studies also show that α-KG alleviates inflammation and oxidative stress[38,39]. We did not find alterations of pro-inflammatory cytokines in plasma, it might be due to the lack of hyperinflammation in *Jak2* V617F transplant mice. Interestingly, although inflammatory cytokine levels remain unaffected, monocytes counts decreases quickly after α-KG treatment in *Jak2* V617F transplant mice. Our results, along with a recent report, supported that monocytes activation are inihibited by α-KG, and monocytes might participate in the impact of α-KG on MPN[23]. The mechanism, mode of action, and effectiveness of α-KG may be cell type-specific and context-dependent. The delivery method, format and tittering of α-KG requires further research for optimization.

In summary, our data demonstrated a previously unrecognized metabolic disorder in platelets that might contribute to hyperreactivity in MPN patients. We also provide evidence for α-KG and mTOR signaling pathway as novel therapeutic approaches against MPN, targeting both platelet hyperreactivity and monocyte-driven inflammation.

MATERIALS AND METHODS

Cell culture

MEG-01 (ATCC) and UKE-1 (Coriell Institute) cells were cultured in RPMI 1640 Medium ATCC modification and RPMI 1640 Medium (ThermoFisher), respectively, supplemented with 10% fetal bovine serum (FBS) and 1% penicillin/streptomycin. All cell lines were maintained at 37°C and 5% CO2 and regularly tested for mycoplasma.

Patient samples

Patient and healthy individual control peripheral blood (PB) or bone marrow (BM) samples were obtained with written consent according to a protocol approved by the Washington University Human Studies Committee (WU no. 01-1014). Mononuclear cells (PBMC or BMMC) were obtained by Ficoll gradient extraction and cryopreserved according to standard procedures. Additional BMMCs were purchased from STEMCELL Technologies (Vancouver, Canada). Lists of patient samples utilized in this study were provided in Table 1 and Table3-6.

Blood collection and platelet isolation from human

Whole blood was drawn into 4.5 mL tubes containing buffered sodium citrate in accordance with an Institutional Review Board-approved protocol at Washington University in St. Louis. Transfer blood into 15ml tube with the addion of 10% (v/v) prewarmed citrate-dextrose solution (ACD). Platelet-rich plasma (PRP) was separated from the other cellular components of blood by centrifugation for at 250g for 20 min without brake and then carefully withdrawn using a plastic Pasteur pipette without disturbing buffy coat. Prostaglandin E1 (PGE1) was added to PRP to a final concentration of 1 μM to prevent aggregation and then spun again for 10 min at 1000 g without brake. The platelet pellet was then carefully washed with 5 mL of Tyrode's-ACD (9 parts of Modified Tyrode's buffer and 1 part of ACD in the presence of PGE1) and spun for 5 min at 700 g. The resultant pellet was gently resuspended in Modified Tyrode's buffer (129 mM NaCl, 0.34 mM Na2HPO4, 2.9 mM KCl, 12 mM NaHCO3, 20 mM HEPES, 5 mM glucose, 1 mM MgCl2; pH 7.3) and adjusted to a count of 3 x 10^8 platelets/ml.

PLA and platelet activation analysis by flow cytometry

PLA were tested as previously described[40]. Blood samples were diluted 5-fold by adding HEPES buffer (145 mM NaCl, 5 mM KCl, 1 mM MgSO4, 0.5 mM NaH2PO4, 5 mM glucose, 10 mM HEPES/Na) within 30 minutes of collection. Diluted blood samples were incubated with PerCP-conjugated CD61 and Pacific Blue-conjugated anti-CD45 mAb for PLA analysis. Samples were also stained with APC-conjugated anti-CD62P mAb for platelet CD62P expression analysis. Samples were stained for 10 min at room temperature. For platelet activation, 1 μM TRAP6 or 5 μg/ml collagen stimulation was added simultaneously with antibody staining. Next, samples were fixed with 1.5 % paraformaldehyde, followed by dilution of 4.6-fold with distilled water for red cell lysis. Samples were analyzed by flow cytometry.

Platelet aggregation assay

Light transmission aggregometry of washed human platelets (300 x 10^3/μl) was performed in PAP-8E platelet aggregometer (Biodata corporation). Aggregations were induced with TRAP6 or collagen as indicated in each experiment.

scRNA-seq and analysis

All MPN patients in the cohort were recruited at the Hematology Department of Washington University School of Medicine in St. Louis. Sample processing were performed as previously published[41]. Chromium Next GEM Single cell 3′ Reagent v3.1 (Dual Index) was used for GEM Generation, barcoding and cDNA library preparation per manufacturer's guidelines, and cDNA was sequenced using the 10X Genomics Single-cell RNA-Seq platform at the Genome Technology Access Center at the McDonnell Genome Institute of Washington University in St. Louis. scRNA-seq analysis details are provided in Supplemental Methods.

Sample preparation for metabolomics and proteomics analysis

Washed platelets were isolated as described above without adding glucose or other nutrients in Modified Tyrode's buffer. 3 x 10^8 platelets were carefully washed with PBS for twice and flash frozen with liquid nitrogen. Metabolomics were performed as previously published and details are provided in Supplemental Methods[42].

Seahorse assay

Bioenergetics of washed platelets (20 × 10^6/well) were determined by Seahorse XFe96 (Agilent Technologies) as previously described[43]. After measurement of basal OCR, OCR due to proton leak was determined by oligomycin A (2.5 μM) treatment. Maximal uncoupled OCR was measured by the addition of the uncoupler carbonyl cyanide p-(trifluoro-methoxy) phenyl-hydrazone (FCCP; 0.5 μM). Nonmitochondrial OCR (defined as the OCR of all cellular processes excluding mitochondrial respiration) was measured in the presence of Rotenone/antimycin A (1 μM). In a subset of samples, TRAP6 (20 μM) was added before oligomycin A to measure TRAP6-stimulated OCR. In another subset of samples, platelets were pre-incubation with octyl-α-KG (200 μM) for one hour to determine the effects of α-KG on platelet bioenergetics.

Western Blot

Washed platelets were lysed with RIPA buffer (Thermo Fisher Scientific) with the existence of protease and phosphatase inhibitor cocktail (Thermo Fisher Scientific) and quantified using Bradford assay (Thermo Fisher Scientific). 20 μg boiled protein were loaded for detection as previously published[44].

Platelet adhesion and spreading assay

Platelets were isolated from *Jak2* V617F knock-in mice by sequential centrifuges. Platelets were incubated with 250 μM Octyl-α-KG at 37°C or DMSO for one hour followed by 100 μM PAR-4 agonist peptide for 5 minutes. Treated platelets were incubated on fibrinogen-coated coverslips for 45 minutes at 37°C in wells of 24-well plate. Coverslips were washed three times with PBS, fixed with paraformaldehyde, permeabilized with 0.1% Triton X-100 and mounted with VECTASHIELD antifade mounting medium with phalloidin (Vector laboratories) and imaged using Nikon A1Rsi confocal microscope and NIS-Elements AR software. Number and area of attached platelets on the coverslips were quantified with CellProfiler software (n = 9). Data are mean ± SD.

Colony forming unit (CFU) assays

CFU assays were performed in semisolid culture using Methocult M3434 (StemCell Technologies, Vancouver, BC, Canada), containing IL-3, IL-6, SCF and EPO. Sorted cKIT+ cells from wt and *Jak2* V617F knock-in mice were seeded at 1000 cells/ml with or without 250 μM Octyl-α-KG in triplicate. Colonnies were counted 14 days post-seeding.

MK differentiation and proplatelet formation

CD34+ cells were sorted from MPN patients and normal individuals cryopreserved BMMCs with MicroBead (Miltenyi Biotec). 2 x 10^4 sorted cells were plated in triplicate in serum-free media containing StemSpan™ Megakaryocyte Expansion Supplement (STEMCELL Technologies) for 10-12 days. Media were replaced every 5 days. Megakaryocyte cell surface markers, including FITC-conjugated CD41 and PerCP-conjugated CD61, were measured by flow cytometry. MEG-01 cells were treated with 10 ng/mL phorbol 12-myristate 13-acetate (PMA) to induce MK differentiation[45].

In vivo models

All procedures were conducted in accordance with the Institutional Animal Care and Use Committee of Washington University.

Normal mice

Regular water or 1% dietary α-KG was administered to 7 week-old C57BL/6 CD45.2 mice. Mice were treated for four weeks and peripheral blood was collected every week for hemavet analysis.

Jak2 V617F model

cKIT+ cells from CD45.2 *Jak2* V617F donor mice were transplanted into CD45.1 lethally irradiated recipient mice as previously published and details are provided in Supplemental Methods. Two weeks after transplant, Mice were supplemented with regular water or 1% dietary α-KG for 6 weeks. Peripheral blood was collected every other week for hemavet tests and. Mice were sacrificed at endpoint, and body, spleen, and liver weights were recorded. Bone marrow samples were collected for flow cytometry and bulk RNA-seq analysis. Femur bones were collected for hematoxylin and eosin staining.

For platelet activation experiments, *Jak2* V617F mice were supplemented with regular water (n = 7) or 2% α-KG (n = 7) for one week. Peripheral blood was collected for platelet activation analysis as described above.

Statistics

Statistical analyses were performed using GraphPad Prism (San Diego, CA) and R software. Two-tailed Student's t test, Mann Whitney U test, two-way ANOVA and Pearson correlations were performed as indicated. All measurements were taken from distinct samples. All relevant assays were performed independently at least 3 times.

Data availability

Bulk RNA-sequencing, scRNA-seq data, and mass cytometry data will be made publicly available upon publication.

ACKNOWLEDGEMENTS

This work was supported by NIH grants R01HL134952 (S.T.O.). Technical support was provided by the Alvin J. Siteman Cancer Center Tissue Procurement Core Facility, Flow Cytometry Core, and Immunomonitoring Laboratory, which are supported by NCI Cancer Center

Support Grant P30CA91842. The Immunomonitoring Laboratory is also supported by the Andrew M and Jane M Bursky Center for Human Immunology and Immunotherapy Programs. We thank D. Bender, R. Lin, and K. Link for assistance with mass cytometry experiments. Bulk RNA-seq and scRNA-seq were performed at Genome Technology Access Center core at the McDonnell Genome Institute (GTAC@MGI). We thank Mary Fulbright for assistance with mouse colony management.

AUTHOR CONTRIBUTIONS

F.H., A.B.B.L., T.K., A.L. and L.Y. performed experiments. K.B., N,M.L., D.A.F and M.F. provided technical support. M.J.C. coordinated clinical sample collection. A.D.A. performed proteomics and metabolomics experiments. F.H., S.M.S., J.D.P., and S.T.O. designed and supervised the experiments. F.H., J.D.P., and S.T.O. wrote the manuscript. All authors read and approved of the manuscript.

COMPETING INTERESTS

S.T.O. has served as a consultant for Kartos Therapeutics, CTI BioPharma, Celgene/Bristol Myers Squibb, Disc Medicine, Blueprint Medicines, PharmaEssentia, Constellation, Geron, Abbvie, Sierra Oncology, and Incyte. All other authors disclose no competing interests.

SUPPLEMENTARY METHODS

scRNA-seq analysis

scRNA-Seq data were initially processed by the Cell Ranger pipeline (v2.1.0) from 10 X Genomics using the human reference genome (GrCH38). The generated count matrices were then analyzed with the Seurat package in R. Read counts were normalized to library size, scaled by 10,000, log transformed, and filtered based on the following criteria: cells with less than 250 genes detected, proportion of the UMIs mapped to mitochondrial genes over 0.1 were excluded from analysis; genes detected in less than 10 cells were also excluded. Cell-cell variation in gene expression driven by the number of detected molecules and mitochondrial gene expression were regressed out using linear regression. Dimensionality reduction, PCA, UMAP projection, and graph-based clustering analysis were then performed. Marker genes for each cluster were identified with Wilcoxon rank sum test. Gene set enrichment analysis of DEGs was run using fgsea and the Hallmark gene set from msigdbr. Platelet activation gene set was downloaded from MSIGDB (www.gsea-msigdb.org)[46,47].

Metabolomics

Metabolites were extracted from frozen platelet pellets at 4 x 10^8/mL by vigorous vortexing in the presence of ice cold 5:3:2 MeOH:MeCN:water (v/v/v) for 30 min at 4°C. Plasma samples were thawed on ice then a 20 µL aliquot was treated with 480 µL of the aforementioned solution then vortexed for 30 min at 4°C. Supernatants were clarified by centrifugation (10 min, 12,000 g, 4°C). The resulting extracts were analyzed (10 µL per injection for platelets, 20 µL per injection for plasma) by ultra-high-pressure liquid chromatography coupled to mass spectrometry (UHPLC-MS - Vanquish and Q Exactive, Thermo). Metabolites were resolved on a Kinetex C18 column

(2.1 x 150 mm, 1.7 µm) using a 5-minute gradient method exactly as previously described[48]. Following data acquisition, .raw files were converted to .mzXML using RawConverter then metabolites assigned and peaks integrated using Maven (Princeton University) in conjunction with the KEGG database and an in-house standard library. Quality control was assessed as using technical replicates run at beginning, end, and middle of each sequence as previously described. Data were adjusted by protein quantity from proteomics. For data analysis, the peak intensities were normalized by median, log transformed and Pareto scaled on MetaboAnalyst website (www.metaboanalyst.ca). Processed data were analyzed with R using limma package.

Proteomics

The samples were processed using the S-Trap filter (Protifi, Huntington, NY) according to the manufacturer's procedure. Briefly, a pellet after metabolomics extraction was solubilized in 50 µl of 5% SDS. Samples were reduced with 10 mM DTT at 55°C for 30 min, cooled to room temperature, and then alkylated with 25 mM iodoacetamide in the dark for 30 min. Next, a final concentration of 1.2% phosphoric acid and then six volumes of binding buffer (90% methanol; 100 mM triethylammonium bicarbonate, TEAB; pH 7.1) were added to each sample. After gentle mixing, the protein solution was loaded to a S-Trap filter, spun at 1,000 x g for 1 min, and the flow-through collected and reloaded onto the filter. This step was repeated three times, and then the filter was washed with 200 µL of binding buffer 3 times. Finally, 1 µg of sequencing-grade trypsin (Promega) and 150 µL of digestion buffer (50 mM TEAB) were added onto the filter and digested carried out at 37°C for 6 h. To elute peptides, three stepwise buffers were applied, with 100 µL of each with one more repeat, including 50 mM TEAB, 0.2% formic acid in H2O, and 50% acetonitrile and 0.2% formic acid in H2O. The peptide solutions were pooled, lyophilized and resuspended in 100 µl of 0.1% FA.

A 20 µl of each sample was loaded onto individual Evotips for desalting and then washed with 20 µL 0.1% FA followed by the addition of 100 µL storage solvent (0.1% FA) to keep the Evotips wet until analysis. The Evosep One system (Evosep, Odense, Denmark) was used to separate peptides on a Pepsep column, (150 µm inter diameter, 15 cm) packed with ReproSil C18 1.9 µm, 120A resin. The system was coupled to the timsTOF Pro mass spectrometer (Bruker Daltonics, Bremen, Germany) via the nano-electrospray ion source (Captive Spray, Bruker Daltonics).

The mass spectrometer was operated in PASEF mode. The ramp time was set to 100 ms and 10 PASEF MS/MS scans per topN acquisition cycle were acquired. MS and MS/MS spectra were recorded from *m/z* 100 to 1700. The ion mobility was scanned from 0.7 to 1.50 Vs/cm2. Precursors for data-dependent acquisition were isolated within ± 1 Th and fragmented with an ion mobility-dependent collision energy, which was linearly increased from 20 to 59 eV in positive mode. Low-abundance precursor ions with an intensity above a threshold of 500 counts but below a target value of 20000 counts were repeatedly scheduled and otherwise dynamically excluded for 0.4 min.

MS/MS spectra were extracted from raw data files and converted into .mgf files using MS Convert (ProteoWizard, Ver. 3.0). Peptide spectral matching was performed with Mascot (Ver. 2.6) against the Uniprot human database. Mass tolerances were +/- 15 ppm for parent ions, and +/- 0.4 Da for fragment ions. Trypsin specificity was used, allowing for 1 missed cleavage. Met oxidation, protein N-terminal acetylation and peptide N-terminal pyroglutamic acid formation were set as variable modifications with Cys carbamidomethylation set as a fixed modification.

Scaffold (version 5.0, Proteome Software, Portland, OR, USA) was used to validate MS/MS based peptide and protein identifications. Peptide identifications were accepted if they could be established at greater than 95.0% probability as specified by the Peptide Prophet algorithm. Protein identifications were accepted if they could be established at greater than 99.0% probability and contained at least two identified unique peptides. Data were analyzed with R using DEP package. Normalized data were input for gene set enrichment analysis.

Mass cytometry (CyTOF)

Whole blood was drawn into 4.5 mL tubes containing sodium heparin in accordance with an Institutional Review Board-approved protocol at Washington University in St. Louis. 200 µl whole blood were incubated with 200 µM Octyl-α-KG or DMSO for 1 hour followed by the stimulation of 10 ng/ml TNFα for 5 min. Add 1 x Proteomic Stabilizer from Smart Tube Inc (1.4ml of Stabilizer per ml of blood), mix gently and incubate for 10 minutes at room temperature. Keep samples at -80°C until it is ready to be stained. Frozen samples were thawn in cold water bath (10°C to 15°C) with agitation of the water for approximately 20 minutes until the samples are fully thawed. Sampels were washed with Thaw-Lyse Buffer to lyse erythrocytes accordingly. Cells were then permeabilized, barcoded, stained with surface marker antibodies, permeabilized with methanol, stained with intracellular antibodies, and resuspended in DNA IR-intercalator. CyTOF experiments were conducted on a CyTOF2 mass cytometry (Fluidigm) with validated antibody panels. Post CyTOF run, cell identities were debarcoded and data was analyzed in Cytobank (cytobank.org). monocytes were gated as follows: CD45+, CD66b-, CD14+. Raw median signal intensities were used for analysis.

FIGURE LEGENDS

Figure 1. Platelets from ET patients show significantly increased p-selectin level and platelet-leukocyte aggregates (PLA) formation. A) Exposure of P-selectin on the surface of platelet was measured by flow cytometry in whole blood using Allophycocyanin (APC)-conjugated CD62P antibody and Peridinin-Chlorophyll-Protein (PerCP)-conjugated CD61 as a platelet marker. B) P-selectin expression (a-granule secretion) is presented as the % positive staining of anti-CD62P antibody at baseline and following 1 µM TRAP6 or 5 µg/ml collagen stimulation. Data are mean ± SD. Statistics were assessed by two-tailed Mann-Whitney U test. C) PLA was measured by flow cytometry in whole blood using the following monoclonal antibodies: Pacific Blue-conjugated CD45 as a leukocyte marker and PerCP-conjugated CD61 as a platelet marker. D) PLA measurements in whole blood at baseline and following 1 µM TRAP6 or 5 µg/ml collagen stimulation. Data are presented as percents of aggregates from the respective leukocyte population. Data are mean ± SD. Statistics were assessed by two-tailed Mann-Whitney U test. E) $\alpha_{IIb}\beta_3$ integrin expression (presented as the % positive staining of anti-PAC-1 antibody) at baseline and following 1 µM TRAP6 or 5 µg/ml collagen stimulation. Data are mean ± SD. Statistics were assessed by two-tailed Mann-Whitney U test. F) Pearson correlation coefficient among platelet markers and parameters. G) Simple linear regression between PLA % and P-selectin % in MPN patients. H) Simple linear regression between PAC-1 % and P-selectin % in MPN patients.

Figure 2. scRNA-seq revealed the activation of platelets and monocytes in peripheral blood from ET patients. A) UMAP plot of cells sequenced from healthy controls (blue) and ET patients (red). B) UMAP plot of cells sequenced from healthy controls (blue) and ET patients (red) with cell type annotations. C) UMAP plot showing platelets clustering with scores for "reactome platelet activation signaling and aggregation" gene set. D) UMAP plot showing platelets from healthy controls (blue) and ET patients (red). E) Violin plots of platelets clusters showing scores for "reactome platelet activation signaling and aggregation" gene set. F) Venn plot showing overlapped genes among differentially expressed genes in platelets from healthy controls (blue), ET patients (red) and genes in "reactome platelet activation signaling and aggregation" gene set (green). G) Dot plot of genes in "reactome platelet activation signaling and aggregation" gene set that overlaped with differentially expressed genes in platelets from healthy controls (0/186) and ET patients (62/686).

Figure 3. Metabolomics analyses showed distinct metabolic phenotypes of platelets from MPN patients. A) Diagram showing sample collection, processing and analysis. B) Principal component analysis (PCA) scores plot of metabolites LC-MS data of platelets from age- and sex-meatched HIs (n = 8) and MPN patients (ET = 12, PV = 7, MF = 9) displayed at 80% confidence region. C) Volcano plot of metabolite changes between HIs and MPN patients. Red dots denote significant ($p < 0.05$) and fold change (>2^0.5) features, Blue dots denote significant ($p < 0.05$) and fold change (<-2^0.5) features. D) The diagram showing steps of glycolysis and TCA cycle and scatter plots of peak areas (arbitrary units after normalization) for several key metabolites. Data are mean ± SD. Statistics were assessed by two-tailed Mann-Whitney U test. E) PCA scores plot of top 500 most variable proteins in protein LC-MS data of platelets from age- and sex-meatched HIs (n = 8) and MPN patients (ET = 12, PV = 7, MF = 9). F) Heatmap of selected proteins from "hallmark mTORC1 signaling", "hallmark OXPHOS" and "hallmark myc targets" gene sets. Columns are reorder based on the results of hierarchical clustering to identify sample correlations. G) GSEA enrichment plots for "mTORC1 signaling" and "Oxidative phosphorylation" gene sets enriched in ET *vs.* HI. H) Western blot of washed platelets from HIs and MPN patients against TOMM20, a mitochondrial marker protein, and human OXPHOS antibody cocktail and quantifications. Data are mean ± SD. Statistics were assessed by two-tailed Mann-Whitney U test.

Figure 4. Platelets from MPN patients displayed bioenergetic alterations, which can be reverted by α-KG supplementation. A) Representative platelet OCR and ECAR profiles from 2 healthy control subjects, a patient with ET and a patient with MF. B) Quantification of basal OCR, ATP production, maximal OCR and spare capacity profiles of washed platelets in HIs (n = 8) and MPN subjects (n = 28, ET = 12, PV = 7, MF = 9). Data are mean ± SD. Statistics were assessed by two-tailed Mann-Whitney U test. C) Representative platelet OCR profiles from a healthy control subject and a patient with ET in the existence of TRAP6 stimulation or not and quantification of post-TRAP6 stimulation OCR profile of washed platelets in HIs and MPN subjects. Data are mean ± SD. Statistics were assessed by two-tailed Mann-Whitney U test. D) Representative platelet OCR and ECAR profiles from a healthy control subject and a patient with ET with the pre-incubation of 500 μM Octyl-α-KG for 1 hour or DMSO. E) Platelet OCR/ECAR ratio from a healthy control subject and a patient with ET with the pre-incubation of 500 μM Octyl-α-KG or DMSO. F) Quantification of individual components of the platelet OCR profile in MPN subjects (n = 5). Data were

normalized to DMSO group set as 1. Data are mean ± SD. Statistics were assessed by two-tailed Mann-Whitney U test.

Figure 5. α-KG inhibited platelet activation through the suppression of ATP synthase. A) Platelets were isolated from peripheral blood of ET patients and and incubated with 200 μM Octyl-α-KG for one hour and stimulated with 1 μM TRAP6 for 5 minutes followed by analysis of P-selectin and αIIbβ3 integrin expression expression on the surface of platelet by flow cytometry. Data are mean ± SD. Statistics were assessed by two-tailed paired t test. B) Washed platelets from *VavCre*/*Jak2 V617F* knock-in mice were incubated with Octyl-α-KG at 37°C for one hour or PAR-4 agonist peptide for 5 minutes followed by placing on fibrinogen-coated coverslips for 45 minutes at 37°C. Coverslips were mounted with VECTASHIELD antifade mounting medium with phalloidin and imaged using Nikon A1Rsi confocal microscope. Number and area of attached platelets on the coverslips were quantified with CellProfiler software (n=9). Data are mean ± SD. Statistics were assessed by two-tailed Mann-Whitney U test. C) Platelets were isolated from peripheral blood of ET patients, incubated with 100 μM (L) or 200 μM (H) Octyl-α-KG for one hour and stimulated with 5 μM TRAP6 followed by platelet aggregation tests in light transmission aggregometry. Maximal aggregation intensity were quantified as mean ± SD. Statistics were assessed by two-tailed paired t test. D) Age- and sex-matched wt and *VavCre/Jak2 V617F* knock-in mice were supplemented with regular water (n= 7) or 2% α-KG (n = 7) for 2 weeks. Platelets were stimulated with thrombin *ex vivo* or not for 1 minute followed by flow cytometry analysis. Data is shown as the ratio (mean ± SD) of P-selectin- and αIIbβ3 integrin-dual positive platelets. Statistics were assessed by Two-tailed Student's t test. E) Washed platelets from ET patients were incubated with 250 μM or 500 μM Octyl-α-KG followed by stimulation with TRAP6 peptides. Platelets were lysed for western blot determination of human p44/42 MAPK, Phospho-p44/42 MAPK, Akt (pan), Phospho-Akt (Ser473), Stat3, Phospho-Stat3 (Tyr705) and Integrin β3. F) Washed platelets from ET patients were incubated with 250 μM Octyl-α-KG followed by stimulation with 5 μM TRAP6 peptides or 5 μg/ml collagen or 20 μM ADP. Platelets were lysed for western blot analysis. G) Washed platelets from ET patients were incubated with 250 μM Octyl-α-KG or 1 μM Oligomycin (Omy) followed by stimulation with TRAP6 peptides. Platelets were lysed for western blot analysis.

Figure 6. α-KG exerts therapeutic impacts on MPN and inhibits megakarypoiesis. A) Schematic of the *JAK2 V617F* knock-in mice. c-KIT+ cells from CD45.2 C57BL/6J mice were isolated and transplanted into CD45.1 C57BL/6J mice. Mice were supplemented with regular water (n= 10) or 1% α-KG in drinking water (n = 10) daily for 6 weeks. B) Spleen weight of transplanted mice normalized to body weight measured at the end of treatments. Data are mean ± SD. Statistics were assessed by Two-tailed Student's t test. C) WBC, platelet count, RBC and lymphocyte ratios of transplanted mice treated with vehicle or α-KG across multiple timepoints. Data are mean ± SD. Statistics were assessed by two-way ANOVA with Dunnett's multiple comparisons test. D) CD34+ hematopoietic stem and progenitor cells were sorted with CD34 MicroBead Kit (Miltenyi Biotec) by autoMACS Pro Separator (Miltenyi Biotec) from bone marrow. $2*10^4$ cells were plated on 6-well plate with StemSpan™ Megakaryocyte Expansion Supplement (100X) for the differentiation of megakaryocytes or StemSpan™ CD34+ Expansion Supplement (10X) for the expansion of CD34+ cells. Cells were cytospinned to slides for fluorescent staining with anti-

Integrin αIIb/ITGA2B/CD41 Antibody (B-9) Alexa Fluor® 488 (Santa Cruz), TRITC-Phalloidin (VECTASHIELD) for F-actin and DAPI for nuclei. E) Sorted CD34+ hematopoietic stem and progenitor cells were cultured with StemSpan™ Megakaryocyte Expansion Supplement (100X) for the differentiation of megakaryocytes with 250 µM Octyl-α-KG or not for 10 days and CD41- and CD61-dual positive cells were determined by flow cytometry. Data are mean ± SD. Statistics were assessed by two-tailed paired t test. F) Percentage of LSK cells of transplanted mice treated with vehicle or α-KG at the end of treatments. Data are mean ± SD. Statistics were assessed by Two-tailed Student's t test. G) Colony-forming unit (CFU) assays were performed with LSK cells from wt and *VavCre/Jak2 V617F* knock-in mice. Colony numbers were counted after 10 days. Data are mean ± SD. Statistics were assessed by Two-tailed Student's t test.

Figure 7. α-KG inhibited monocytes activation and hyperinflammation. A) Plasma from HIs (n = 9) and MPN patients (n = 28) were collected for the determination of 30 biomarkers using V-PLEX Human Cytokine 30-Plex Kit from Meso Scale Discovery. Data are mean ± SD. Statistics were assessed by two-tailed Mann-Whitney U test. B) 0.5M sorted CD14+ monocytes (n = 5) were incubated with Octyl-α-KG or Omy for 8 hours and the supernants were collected for cytokine secretion examination. Data are mean ± SD. Statistics were assessed by two-tailed Mann-Whitney U test. C) Sorted CD14+ monocytes (n = 5) after the incubation with Octyl-α-KG or DMSO were sent for bulk RNA sequencing analysis. The PCA scores plot of the monocytes. D) Barplot of top 5 hallmark pathways with the highest enrichment scores. E) whole blood from MPN patients (n = 6) were incubated with Octyl-α-KG or DMSO for 1 hour followed by the stimulation of TNFα. Samples were processed for the determination of intracellular pathway activities by mass cytometry (CyTOF). Data are mean ± SD. Statistics were assessed by two-tailed paired t test.

SUPPLEMENTARY FIGURE LEGENDS

Figure S1. Analysis of platelet activation, secretion and aggregation A) Platelets were isolated from peripheral blood of HIs and ET patients and and stimulated with TRAP6 or collagen followed by flow cytometry analysis. B) Washed platelets from HIs and MPN patients were subjected for platelet aggregation determination in a Lumi-Aggregometer (Chrono-log Corporation). Data is shown as mean ± SD of maximal aggregation intensity. C) Subgroup analysis of platelet aggregation with different MPN subtypes. D) Subgroup analysis of platelet aggregation with different disease mutations.

Figure S2. scRNA-seq analysis (part1). A) Feature plots of genes for cell type identification. B) Dot plot of top differentially expressed genes for cell type identification. C) Dotplot showing frequency of differernt type of cells in all 8 samples of scRNA-seq. D) GO enrichment analysis of differentially-expressed genes (DEGs) in ET platelets. E) KEGG enrichment analysis of DEGs in ET platelets. F) heatmap showing the distribution of DEGs in GO enrichment pathways. G) Barplot showing top 5 reactome (red fill) and hallmark (no fill) pathways enriched in platelets (ET vs. HI). H) GSEA enrichment plots for "reactome platelet activation signaling and aggregation" gene set enriched in ET vs. HI platelets. I) GSEA enrichment plots for "hallmark IFN-γ response" gene set enriched in ET vs. HI platelets. J) GSEA enrichment plots for "hallmark OXPHOS" gene set enriched in ET vs. HI platelets.

Figure S3. Analysis of GSE2006 microarray between platelets from HIs and ET patients. A) PCA plot of platelet from ET (n = 6) and HIs (n = 5) in GSE2006. B) Volcano plot showing differentially expressed genes (DEG) between HIs and ET patients in platelets in GSE2006. C) Heatmap of top 10 DEGs in HIs and ET patients in GSE2006. D) GSEA enrichment plots for "hallmark OXPHOS" and "reactome platelet activation signaling and aggregation" gene sets enriched in ET vs. HIs in GSE2006.

Figure S4. scRNA-seq analysis (part2). A) UMAP and violin plots showing cell type identification and scores for genes in "hallmark interferon gamma response" gene set (C: ET patients carrying *CALR* mutations; J: ET patients carrying *JAK2* mutation; N: HIs). B) UMAP and violin plots showing cell type identification and scores for genes in "hallmark inflammatory response" gene set. C) UMAP plot showing monocytes from HIs (blue) and ET patients (red) and UMAP plot showing monocytes clustering with scores for "hallmark interferon gamma response" gene set. D) Violin plots of monocytes clusters showing scores for "hallmark interferon gamma response" gene set and PPBP (a marker for platelets) expression levels.

Figure S5. Plasma and washed platelets metabolite LC-MS. A) Heatmap of down- (n = 19) and up-regulated (n = 24) metabolites in platelets between ET and HI ($P<0.05$, $|\text{fold change}| > 1.41$). B) PCA plot of metabolites in plasma from MPN patients and HIs. C) Volcano plot of metabolites in plasma from MPN patients and HIs.

Figure S6. Additional seahorse analysis. A) Seahorse assays were performed on washed platelets from wt and *JAK2 V617F* knock-in mice. B) Correlation analysis of bioenergic parameters in platelets C) Seahorse assays were performed on UKE-1 cells with the incubation of Octyl-α-KG or DMSO.

Figure S7. Effects of α-KG on mouse platelets and cell lines. A) Washed platelets from *JAK2 V617F* knock-in mice were treated with Octyl-α-KG for 1 hour followed by PAR-4-AP stimulation and flow cytometry analysis. B) Short term effects (2 hours) of Octyl-α-KG on mitochondrial membrane potential in MEG-01 and UKE-1 cells determined by JC-1 dye staining and flow cytometry. C) Long term effects (3 days) of Octyl-α-KG on mitochondrial membrane potential in MEG-01 and UKE-1 cells determined by JC-1 dye staining and flow cytometry. D) Effects of Octyl-α-KG on intracellular ATP level in MEG-01 and UKE-1 cells determined by ATPlite Luminescence Assay System (PerkinElmer).

Figure S8. *in vivo* treatment of α-KG inhibited MPN progression. A) HCT%, B and T cell ratios from CD45.2+ cells of transplanted mice treated with vehicle or α-KG across multiple timepoints. Data are mean ± SD. Statistics were assessed by two-way ANOVA with Dunnett's multiple comparisons test. B) Percentage of MPP2 cells of transplanted mice treated with vehicle or α-KG across multiple timepoints. Data are mean ± SD. Statistics were assessed by Two-tailed Student's t test. C) Absolute count and percentage of monocytes of transplanted mice treated with vehicle or α-KG across multiple timepoints. Data are mean ± SD. Statistics were assessed by two-way ANOVA with Dunnett's multiple comparisons test. D) Representative HE staining of femur bones

from mice treated with vehicle or α-KG. E) WBC, PLT, MO count and HCT % from C57BL/6J mice treated with vehicle or α-KG across multiple timepoints. F) PCA scores plot for bulk RNA-seq data of bone marrow from control (n = 5) and 1% α-KG-supplemented mice (n = 5). G) Barplot of top 10 hallmark pathways with the highest GSEA enrichment scores. H) GSEA enrichment plots for "Oxidative phosphorylation", "Heme metabolism" and "mTORc1 signaling" gene sets enriched in control vs. α-KG-supplemented mice. I) Visualization of expression levels of some genes. J) MEG-01 cells were treated with phorbol myristate acetate (PMA) for 2 days with 500 µM Octyl-α-KG or not. The ratio of CD41- and CD61-dual positive cells were determined by flow cytometry with the staining of PerCP-CD61 and FITC-CD41 antibodies and quantified (mean ± SD, n =3). Ploidy analysis was determined by propidium iodide (PI) staining.

TABLES

Table 1. Demographics of HIs and MPN patients for flow cytometry.

	HI (n = 7)	ET (n = 17)	MF (n = 8)
Age	44.1 ± 14.7	55.6 ± 10.7	59.1 ± 7.4
Female %	42.9%	76%	75%
JAK2 mutation	NA	12/17	3/8

Table 2. P value of Pearson's correlations between platelet parameters from ET patients.

	PLT count	P-selectin %	PAC-1 %	Age	PLA %
PLT count		0.228	0.469	0.601	0.474
P-selectin %	0.228		0	0.579	0.003
PAC-1 %	0.469	0		0.608	0.045
Age	0.601	0.579	0.608		0.861
PLA %	0.474	0.003	0.045	0.861	

Table 3. Demographics of the MPN patients for JAK2 and CALR comparison.

	JAK2 (n = 18)	CALR (n = 11)
Age	60.7 ± 13.7	63.5 ± 10.1
Female %	83.3%	45.5%
PLT count	508 ± 238	641 ± 327

Table 4. Demographics of HIs and MPN patients for scRNA-seq.

ID	Age	Sex	Diagnosis	Driver mutation	Medication	PLT count	Thrombosis history
PT158	51	F	ET	JAK2	A	500	N
PT164	69	F	ET	JAK2	H + A	300	Y
PT130	59	F	ET	JAK2	H + A	770	Y
PT139	50	F	ET	CALR	A	838	N

PT153	64	M	ET	CALR	H	923	N
HI105	55	F	NA	NA	NA	375	N
HI108	48	M	NA	NA	NA	349	N
HI111	46	F	NA	NA	NA	338	N

H: hydroxyurea; A: aspirin.

Table 5. Demographics of HIs and MPN patients for platelet and plasma metabolomics and proteomics LC-MS.

	HI (n = 8)	ET (n = 12)	PV (n = 7)	MF (n = 9)
Age	51.5 ± 12.1	57.9 ± 11.2	54.9 ± 7.3	59.7 ± 5.6
Female %	37.5%	58.3%	42.9%	88.9%
JAK2 mutation	NA	8/12	7/7	4/9

Table 6. Demographics of HIs and MPN patients for plasma cytokine screening.

	HI (n = 9)	ET-JAK2 (n = 11)	ET-CALR (n = 11)	MFpET (n = 6)
Age	54.7 ± 20.1	57.5 ± 20.0	58.5 ± 17.6	64.5 ± 7.8
Female %	44.4%	72.7%	45.5%	66.7%

REFERENCES

1. Barbui T, Thiele J, Gisslinger H, et al. The 2016 WHO classification and diagnostic criteria for myeloproliferative neoplasms: document summary and in-depth discussion. *Blood Cancer J*. Feb 9 2018;8doi:ARTN 15

10.1038/s41408-018-0054-y

2. Rungjirajittranon T, Owattanapanich W, Ungprasert P, Siritanaratkul N, Ruchutrakool T. A systematic review and meta-analysis of the prevalence of thrombosis and bleeding at diagnosis of Philadelphia-negative myeloproliferative neoplasms. *BMC Cancer*. Feb 28 2019;19(1):184. doi:10.1186/s12885-019-5387-9
3. Barbui T, Carobbio A, De Stefano V. Thrombosis in myeloproliferative neoplasms during cytoreductive and antithrombotic drug treatment. *Res Pract Thromb Haemost*. Jan 2022;6(1):e12657. doi:10.1002/rth2.12657
4. Hasselbalch HC, Elvers M, Schafer AI. The pathobiology of thrombosis, microvascular disease, and hemorrhage in the myeloproliferative neoplasms. *Blood*. Apr 22 2021;137(16):2152-2160. doi:10.1182/blood.2020008109
5. Duchemin J, Ugo V, Ianotto JC, Lecucq L, Mercier B, Abgrall JF. Increased circulating procoagulant activity and thrombin generation in patients with myeloproliferative neoplasms. *Thromb Res*. Sep 2010;126(3):238-42. doi:10.1016/j.thromres.2010.06.025
6. Panova-Noeva M, Marchetti M, Spronk HM, et al. Platelet-induced thrombin generation by the calibrated automated thrombogram assay is increased in patients with essential thrombocythemia and polycythemia vera. *Am J Hematol*. Apr 2011;86(4):337-42. doi:10.1002/ajh.21974
7. Cella G, Marchetti M, Vianello F, et al. Nitric oxide derivatives and soluble plasma selectins in patients with myeloproliferative neoplasms. *Thromb Haemost*. Jul 2010;104(1):151-6. doi:10.1160/TH09-09-0663
8. Lamrani L, Lacout C, Ollivier V, et al. Hemostatic disorders in a JAK2V617F-driven mouse model of myeloproliferative neoplasm. *Blood*. Aug 14 2014;124(7):1136-45. doi:10.1182/blood-2013-10-530832
9. Hobbs CM, Manning H, Bennett C, et al. JAK2V617F leads to intrinsic changes in platelet formation and reactivity in a knock-in mouse model of essential thrombocythemia. *Blood*. Nov 28 2013;122(23):3787-3797. doi:10.1182/blood-2013-06-501452
10. Fisher DAC, Fowles JS, Zhou A, Oh ST. Inflammatory Pathophysiology as a Contributor to Myeloproliferative Neoplasms. *Front Immunol*. 2021;12:683401. doi:10.3389/fimmu.2021.683401
11. Taus F, Salvagno G, Cane S, et al. Platelets Promote Thromboinflammation in SARS-CoV-2 Pneumonia. *Arterioscler Thromb Vasc Biol*. Dec 2020;40(12):2975-2989. doi:10.1161/ATVBAHA.120.315175
12. Sefer D, Miljic P, Kraguljac-Kurtovic N, et al. Correlation between leukocyte-platelet aggregates and thrombosis in myeloproliferative neoplasms. *Int J Lab Hematol*. Apr 2022;44(2):302-312. doi:10.1111/ijlh.13754
13. Marin Oyarzun CP, Heller PG. Platelets as Mediators of Thromboinflammation in Chronic Myeloproliferative Neoplasms. *Front Immunol*. 2019;10:1373. doi:10.3389/fimmu.2019.01373
14. Marin Oyarzun CP, Glembotsky AC, Goette NP, et al. Platelet Toll-Like Receptors Mediate Thromboinflammatory Responses in Patients With Essential Thrombocythemia. *Front Immunol*. 2020;11:705. doi:10.3389/fimmu.2020.00705
15. Wang L, Wu Q, Fan Z, Xie R, Wang Z, Lu Y. Platelet mitochondrial dysfunction and the correlation with human diseases. *Biochem Soc Trans*. Dec 15 2017;45(6):1213-1223. doi:10.1042/BST20170291

16. Davizon-Castillo P, McMahon B, Aguila S, et al. TNF-alpha-driven inflammation and mitochondrial dysfunction define the platelet hyperreactivity of aging. *Blood*. Aug 29 2019;134(9):727-740. doi:10.1182/blood.2019000200
17. Jensen MK, de Nully Brown P, Lund BV, Nielsen OJ, Hasselbalch HC. Increased circulating platelet-leukocyte aggregates in myeloproliferative disorders is correlated to previous thrombosis, platelet activation and platelet count. *Eur J Haematol*. Mar 2001;66(3):143-51. doi:10.1034/j.1600-0609.2001.00359.x
18. Rotunno G, Mannarelli C, Guglielmelli P, et al. Impact of calreticulin mutations on clinical and hematological phenotype and outcome in essential thrombocythemia. *Blood*. Mar 6 2014;123(10):1552-5. doi:10.1182/blood-2013-11-538983
19. Linke M, Fritsch SD, Sukhbaatar N, Hengstschlager M, Weichhart T. mTORC1 and mTORC2 as regulators of cell metabolism in immunity. *FEBS Lett*. Oct 2017;591(19):3089-3103. doi:10.1002/1873-3468.12711
20. Wu N, Yang M, Gaur U, Xu H, Yao Y, Li D. Alpha-Ketoglutarate: Physiological Functions and Applications. *Biomol Ther (Seoul)*. Jan 2016;24(1):1-8. doi:10.4062/biomolther.2015.078
21. Chin RM, Fu X, Pai MY, et al. The metabolite alpha-ketoglutarate extends lifespan by inhibiting ATP synthase and TOR. *Nature*. Jun 19 2014;510(7505):397-401. doi:10.1038/nature13264
22. Asadi Shahmirzadi A, Edgar D, Liao CY, et al. Alpha-Ketoglutarate, an Endogenous Metabolite, Extends Lifespan and Compresses Morbidity in Aging Mice. *Cell Metab*. Sep 1 2020;32(3):447-456 e6. doi:10.1016/j.cmet.2020.08.004
23. Shrimali NM, Agarwal S, Kaur S, et al. alpha-Ketoglutarate Inhibits Thrombosis and Inflammation by Prolyl Hydroxylase-2 Mediated Inactivation of Phospho-Akt. *EBioMedicine*. Nov 2021;73:103672. doi:10.1016/j.ebiom.2021.103672
24. Hao W, Chang CP, Tsao CC, Xu J. Oligomycin-induced bioenergetic adaptation in cancer cells with heterogeneous bioenergetic organization. *J Biol Chem*. Apr 23 2010;285(17):12647-54. doi:10.1074/jbc.M109.084194
25. Masselli E, Pozzi G, Gobbi G, et al. Cytokine Profiling in Myeloproliferative Neoplasms: Overview on Phenotype Correlation, Outcome Prediction, and Role of Genetic Variants. *Cells*. Sep 21 2020;9(9)doi:10.3390/cells9092136
26. Fisher DAC, Malkova O, Engle EK, et al. Mass cytometry analysis reveals hyperactive NF Kappa B signaling in myelofibrosis and secondary acute myeloid leukemia. *Leukemia*. Sep 2017;31(9):1962-1974. doi:10.1038/leu.2016.377
27. Fisher DAC, Miner CA, Engle EK, et al. Cytokine production in myelofibrosis exhibits differential responsiveness to JAK-STAT, MAP kinase, and NFkappaB signaling. *Leukemia*. Aug 2019;33(8):1978-1995. doi:10.1038/s41375-019-0379-y
28. Arellano-Rodrigo E, Alvarez-Larran A, Reverter JC, Villamor N, Colomer D, Cervantes F. Increased platelet and leukocyte activation as contributing mechanisms for thrombosis in essential thrombocythemia and correlation with the JAK2 mutational status. *Haematologica*. Feb 2006;91(2):169-75.
29. Falanga A, Marchetti M, Vignoli A, Balducci D, Barbui T. Leukocyte-platelet interaction in patients with essential thrombocythemia and polycythemia vera. *Exp Hematol*. May 2005;33(5):523-30. doi:10.1016/j.exphem.2005.01.015
30. Robertson B, Urquhart C, Ford I, et al. Platelet and coagulation activation markers in myeloproliferative diseases: relationships with JAK2 V6I7 F status, clonality, and antiphospholipid antibodies. *J Thromb Haemost*. Aug 2007;5(8):1679-85. doi:10.1111/j.1538-7836.2007.02626.x
31. Trappenburg MC, van Schilfgaarde M, Marchetti M, et al. Elevated procoagulant microparticles expressing endothelial and platelet markers in essential thrombocythemia. *Haematologica*. Jul 2009;94(7):911-8. doi:10.3324/haematol.13774

32. Alvarez-Larran A, Arellano-Rodrigo E, Reverter JC, et al. Increased platelet, leukocyte, and coagulation activation in primary myelofibrosis. *Ann Hematol*. Apr 2008;87(4):269-76. doi:10.1007/s00277-007-0386-3
33. Shen Z, Du W, Perkins C, et al. Platelet transcriptome identifies progressive markers and potential therapeutic targets in chronic myeloproliferative neoplasms. *Cell Rep Med*. Oct 19 2021;2(10):100425. doi:10.1016/j.xcrm.2021.100425
34. Zhan H, Ciano K, Dong K, Zucker S. Targeting glutamine metabolism in myeloproliferative neoplasms. *Blood Cells Mol Dis*. Oct 2015;55(3):241-7. doi:10.1016/j.bcmd.2015.07.007
35. McKenney AS, Lau AN, Somasundara AVH, et al. JAK2/IDH-mutant-driven myeloproliferative neoplasm is sensitive to combined targeted inhibition. *J Clin Invest*. Feb 1 2018;128(2):789-804. doi:10.1172/JCI94516
36. Rao TN, Hansen N, Hilfiker J, et al. JAK2-mutant hematopoietic cells display metabolic alterations that can be targeted to treat myeloproliferative neoplasms. *Blood*. Nov 21 2019;134(21):1832-1846. doi:10.1182/blood.2019000162
37. Carey BW, Finley LW, Cross JR, Allis CD, Thompson CB. Intracellular alpha-ketoglutarate maintains the pluripotency of embryonic stem cells. *Nature*. Feb 19 2015;518(7539):413-6. doi:10.1038/nature13981
38. Mailloux RJ, Singh R, Brewer G, Auger C, Lemire J, Appanna VD. Alpha-ketoglutarate dehydrogenase and glutamate dehydrogenase work in tandem to modulate the antioxidant alpha-ketoglutarate during oxidative stress in Pseudomonas fluorescens. *J Bacteriol*. Jun 2009;191(12):3804-10. doi:10.1128/JB.00046-09
39. Ali R, Mittal G, Sultana S, Bhatnagar A. Ameliorative potential of alpha-ketoglutaric acid (AKG) on acute lung injuries induced by ammonia inhalation in rats. *Exp Lung Res*. Nov 2012;38(9-10):435-44. doi:10.3109/01902148.2012.721859
40. Nagasawa A, Matsuno K, Tamura S, Hayasaka K, Shimizu C, Moriyama T. The basis examination of leukocyte-platelet aggregates with CD45 gating as a novel platelet activation marker. *Int J Lab Hematol*. Oct 2013;35(5):534-41. doi:10.1111/ijlh.12051
41. Fisher MH, Kirkpatrick GD, Stevens B, et al. ETV6 germline mutations cause HDAC3/NCOR2 mislocalization and upregulation of interferon response genes. *JCI Insight*. Sep 17 2020;5(18)doi:10.1172/jci.insight.140332
42. D'Alessandro A, Thomas KA, Stefanoni D, et al. Metabolic phenotypes of standard and cold-stored platelets. *Transfusion*. Jun 2020;60 Suppl 3(Suppl 3):S96-S106. doi:10.1111/trf.15651
43. Nguyen QL, Corey C, White P, et al. Platelets from pulmonary hypertension patients show increased mitochondrial reserve capacity. *JCI Insight*. Mar 9 2017;2(5):e91415. doi:10.1172/jci.insight.91415
44. He F, Borcherds W, Song T, et al. Interaction between p53 N terminus and core domain regulates specific and nonspecific DNA binding. *Proc Natl Acad Sci U S A*. Apr 30 2019;116(18):8859-8868. doi:10.1073/pnas.1903077116
45. Schlinker AC, Duncan MT, DeLuca TA, Whitehead DC, Miller WM. Megakaryocyte Polyploidization and Proplatelet Formation in Low-Attachment Conditions. *Biochem Eng J*. Jul 15 2016;111:24-33. doi:10.1016/j.bej.2016.03.001
46. Subramanian A, Tamayo P, Mootha VK, et al. Gene set enrichment analysis: a knowledge-based approach for interpreting genome-wide expression profiles. *Proc Natl Acad Sci U S A*. Oct 25 2005;102(43):15545-50. doi:10.1073/pnas.0506580102
47. Liberzon A, Birger C, Thorvaldsdottir H, Ghandi M, Mesirov JP, Tamayo P. The Molecular Signatures Database (MSigDB) hallmark gene set collection. *Cell Syst*. Dec 23 2015;1(6):417-425. doi:10.1016/j.cels.2015.12.004

48. Nemkov T, Reisz JA, Gehrke S, Hansen KC, D'Alessandro A. High-Throughput Metabolomics: Isocratic and Gradient Mass Spectrometry-Based Methods. *Methods Mol Biol*. 2019;1978:13-26. doi:10.1007/978-1-4939-9236-2_2

Figure 1

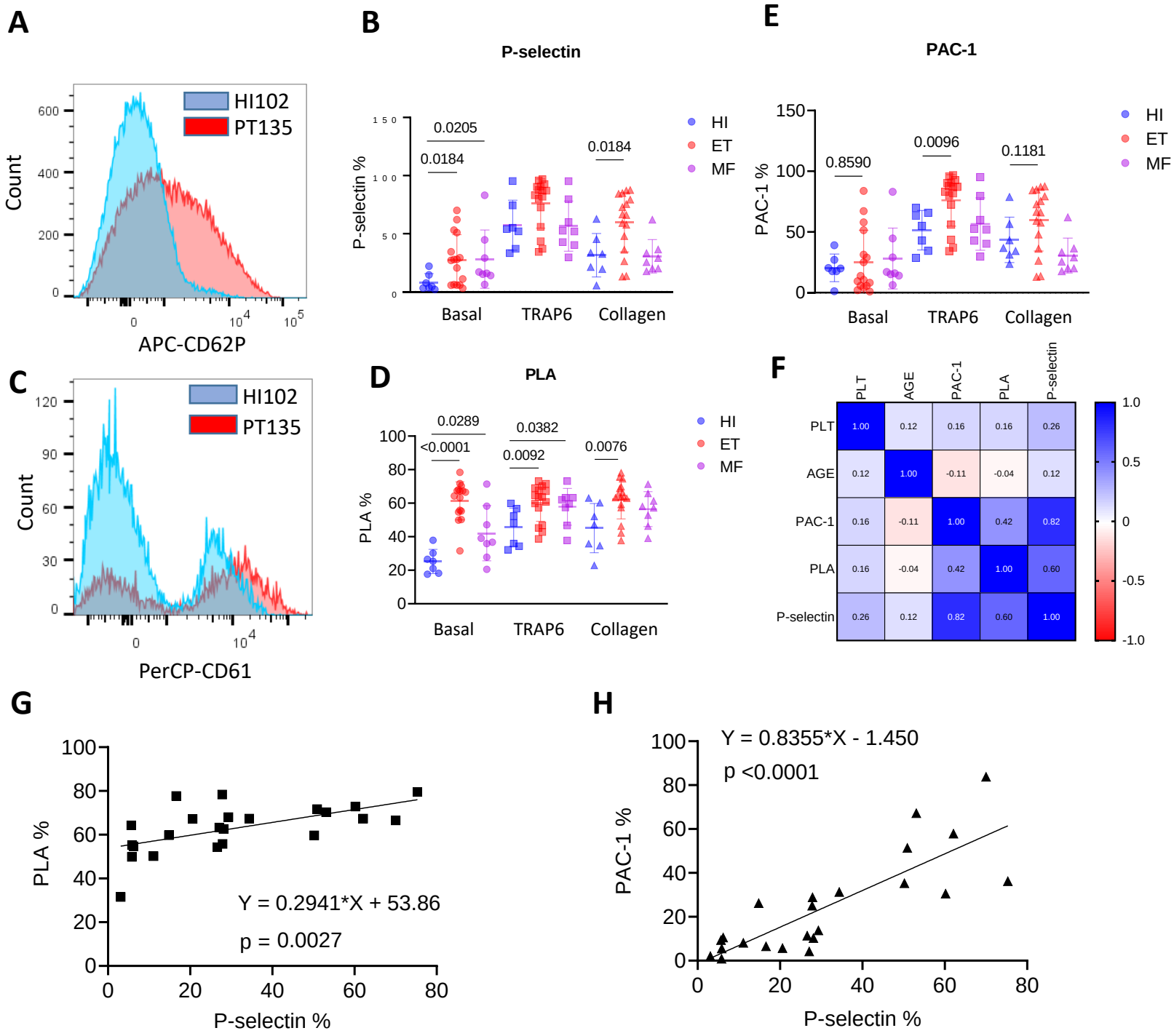
A
HI102
PT135
Count
APC-CD62P
B
P-selectin
P-selectin %
0.0205
0.0184
0.0184
Basal
TRAP6
Collagen
HI
ET
MF
E
PAC-1
PAC-1 %
0.8590
0.0096
0.1181
C
PerCP-CD61
D
PLA
PLA %
0.0289
<0.0001
0.0382
0.0092
0.0076
F
PLT
AGE
PAC-1
PLA
P-selectin
G
Y = 0.2941*X + 53.86
p = 0.0027
H
Y = 0.8355*X - 1.450
p <0.0001

Figure 2

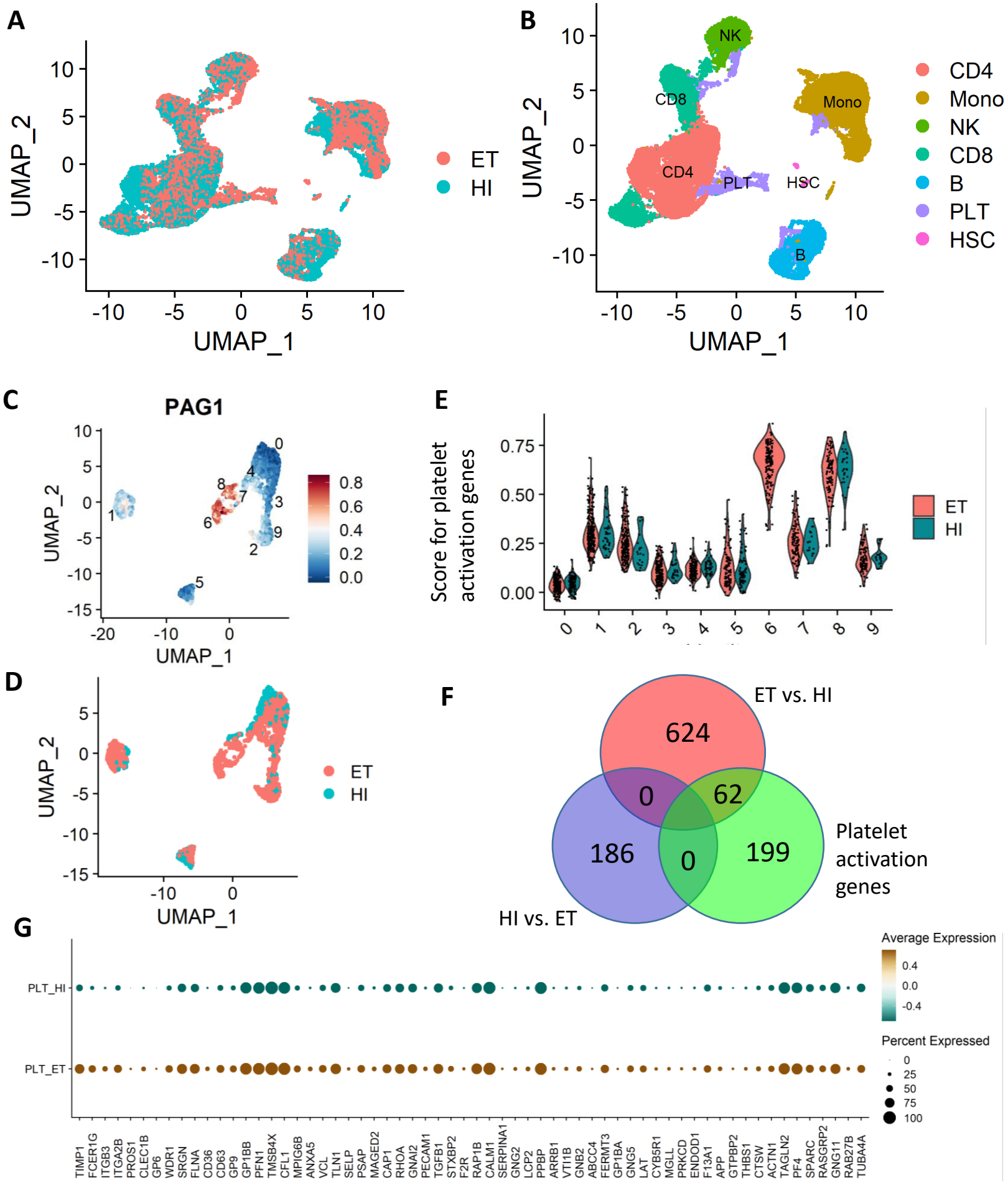
A
UMAP_2
UMAP_1
ET
HI
B
NK
CD8
Mono
CD4
PLT
HSC
B
CD4
Mono
NK
CD8
B
PLT
HSC
C
PAG1
0.8
0.6
0.4
0.2
0.0
D
ET
HI
E
Score for platelet activation genes
ET
HI
F
ET vs. HI
624
0
62
186
0
199
Platelet activation genes
HI vs. ET
G
PLT_HI
PLT_ET
Average Expression
Percent Expressed
TIMP1 FCER1G ITGB3 ITGA2B PROS1 CLEC1B GP6 WDR1 SRGN FLNA CD36 CD63 GP9 GP1BB PFN1 TMSB4X CFL1 MPIG6B ANXA5 VCL TLN1 SELP PSAP MAGED2 CAP1 RHOA GNAI2 PECAM1 TGFB1 STXBP2 F2R RAP1B CALM1 SERPINA1 GNG2 LCP2 PPBP ARRB1 VTI1B GNB2 ABCC4 FERMT3 GP1BA GNG5 LAT CYB5R1 MGLL PRKCD ENDOD1 F13A1 APP GTPBP2 THBS1 CTSW ACTN1 TAGLN2 PF4 SPARC RASGRP2 GNG11 RAB27B TUBA4A

Figure 3

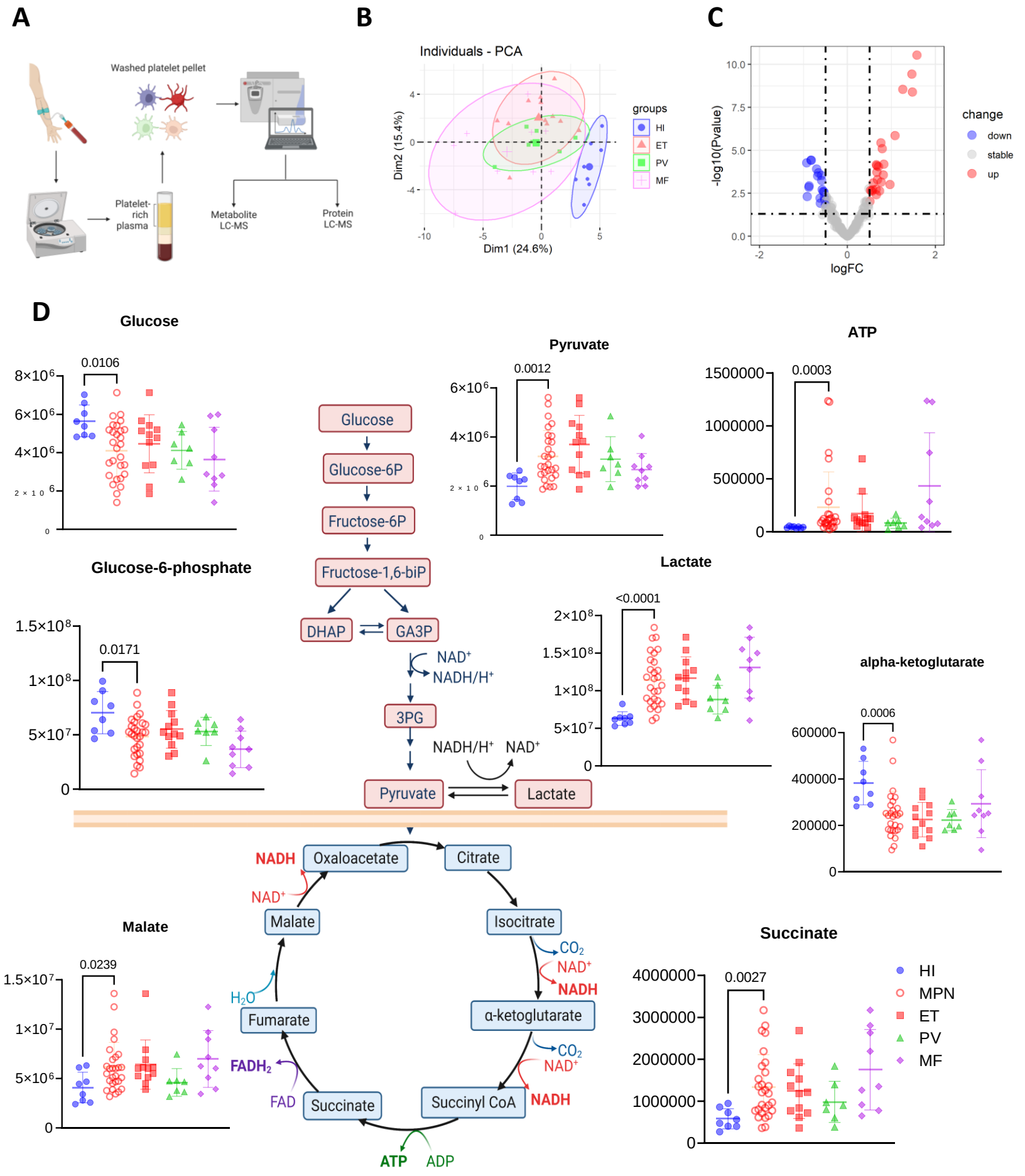
A
Washed platelet pellet
Platelet-rich plasma
Metabolite LC-MS
Protein LC-MS
B
Individuals - PCA
Dim1 (24.6%)
Dim2 (15.4%)
groups
HI
ET
PV
MF
C
-log10(Pvalue)
logFC
change
down
stable
up
D
Glucose
0.0106
Pyruvate
0.0012
ATP
0.0003
Glucose-6-phosphate
0.0171
Lactate
<0.0001
alpha-ketoglutarate
0.0006
Malate
0.0239
Succinate
0.0027
HI
MPN
ET
PV
MF
Glucose
Glucose-6P
Fructose-6P
Fructose-1,6-biP
DHAP
GA3P
NAD+
NADH/H+
3PG
NADH/H+
NAD+
Pyruvate
Lactate
NADH
Oxaloacetate
Citrate
NAD+
Malate
Isocitrate
CO2
NAD+
NADH
H2O
Fumarate
α-ketoglutarate
CO2
NAD+
FADH2
FAD
Succinate
Succinyl CoA
NADH
ATP
ADP

Figure 3

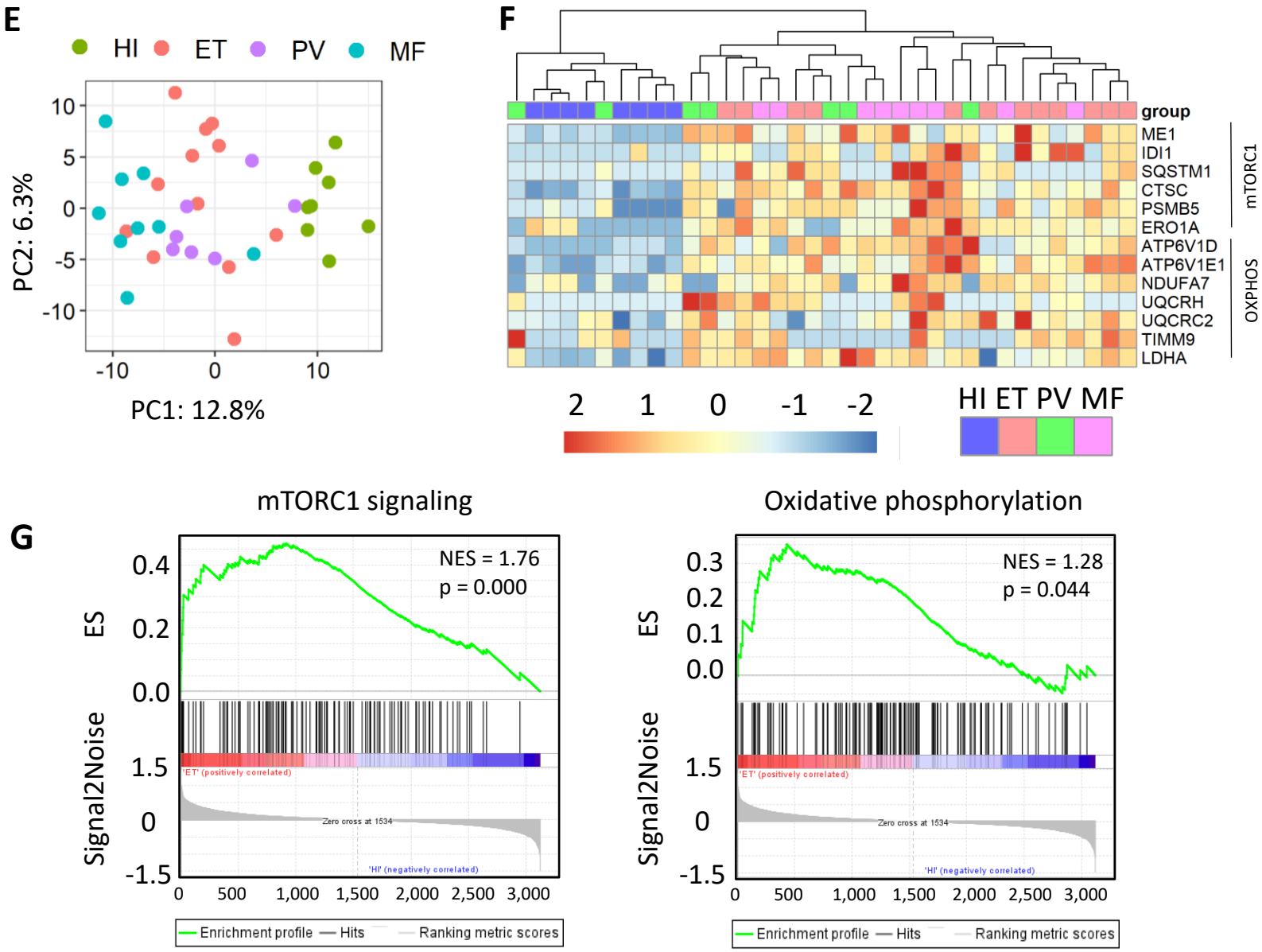
E
HI
ET
PV
MF
PC2: 6.3%
PC1: 12.8%
F
group
ME1
IDI1
SQSTM1
CTSC
PSMB5
ERO1A
ATP6V1D
ATP6V1E1
NDUFA7
UQCRH
UQCRC2
TIMM9
LDHA
mTORC1
OXPHOS
2 1 0 -1 -2
HI ET PV MF
G
mTORC1 signaling
NES = 1.76
p = 0.000
Oxidative phosphorylation
NES = 1.28
p = 0.044
ES
Signal2Noise
Enrichment profile
Hits
Ranking metric scores

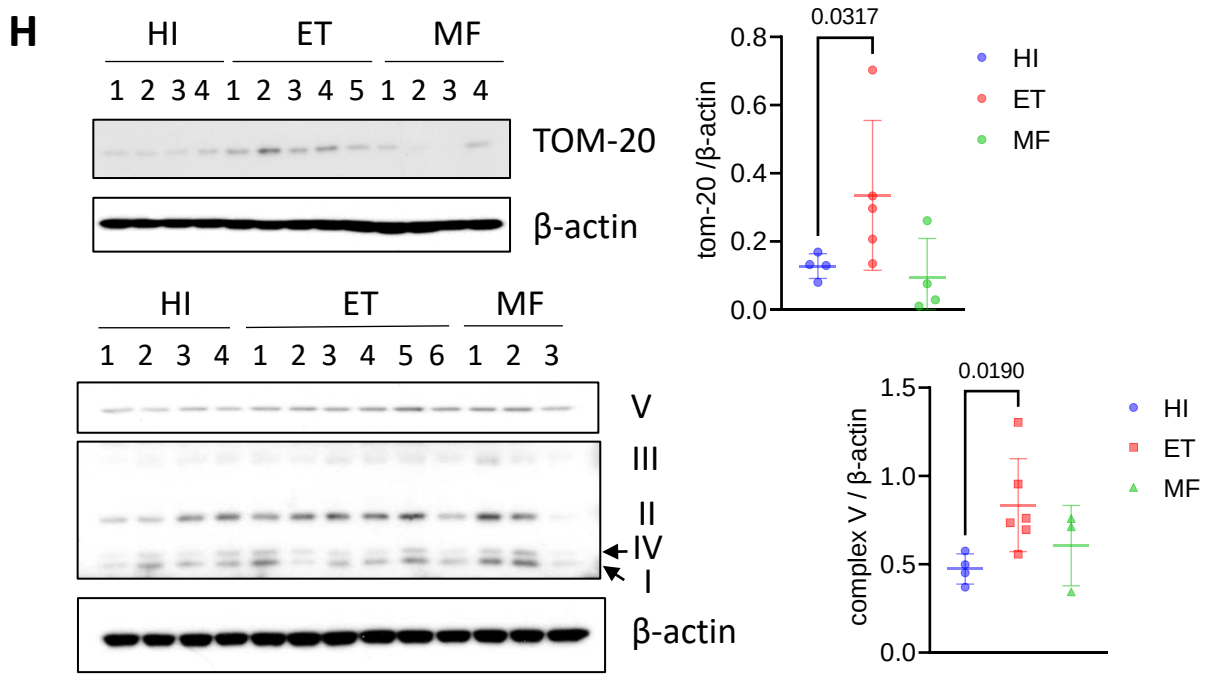
H
HI
ET
MF
TOM-20
β-actin
0.0317
tom-20 /β-actin
V
III
II
IV
I
β-actin
0.0190
complex V / β-actin

Figure 4

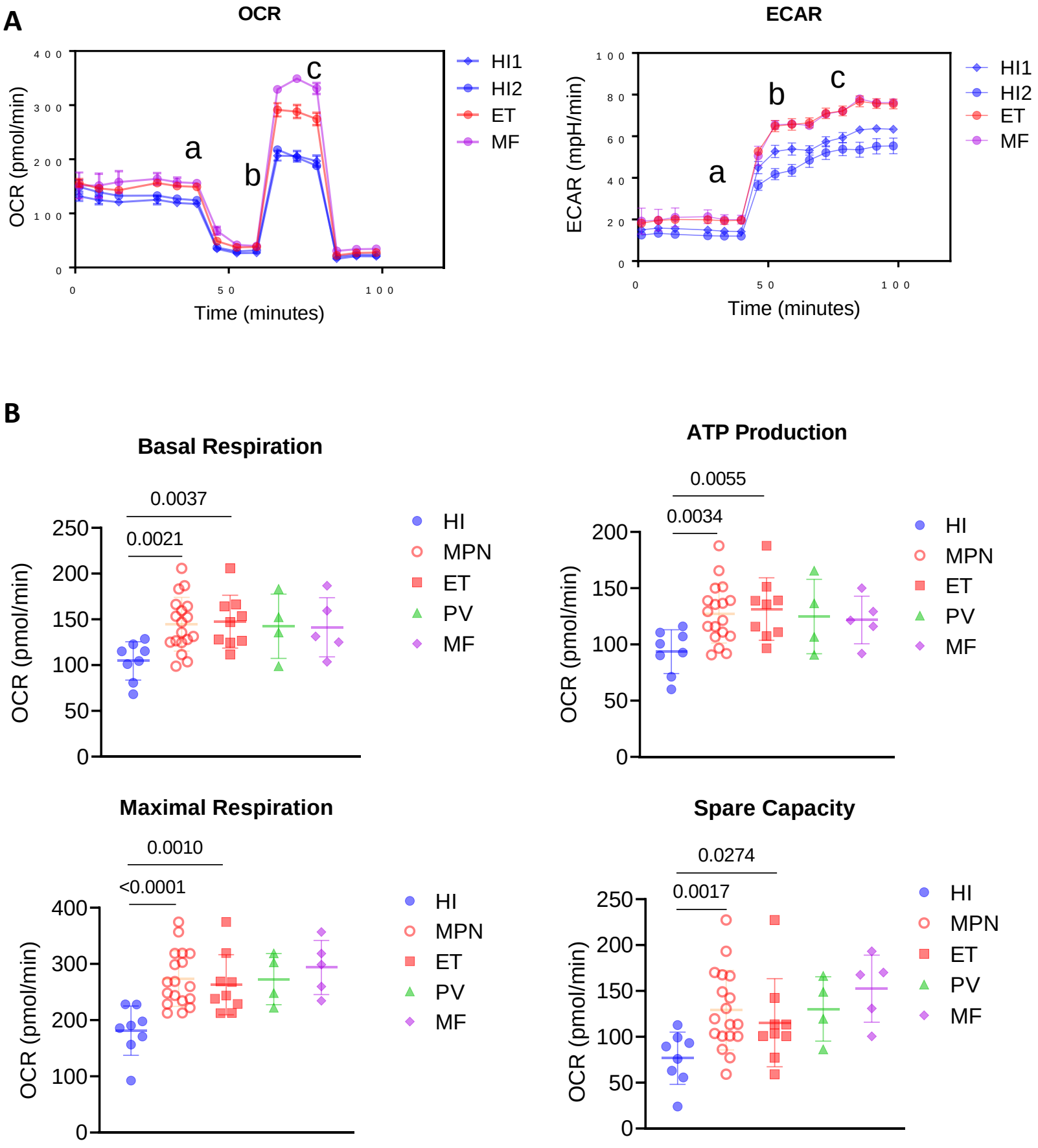
A
OCR
OCR (pmol/min)
Time (minutes)
a
b
c
HI1
HI2
ET
MF
ECAR
ECAR (mpH/min)
Time (minutes)
B
Basal Respiration
0.0037
0.0021
ATP Production
0.0055
0.0034
Maximal Respiration
0.0010
<0.0001
Spare Capacity
0.0274
0.0017
OCR (pmol/min)
HI
MPN
ET
PV
MF

Figure 4

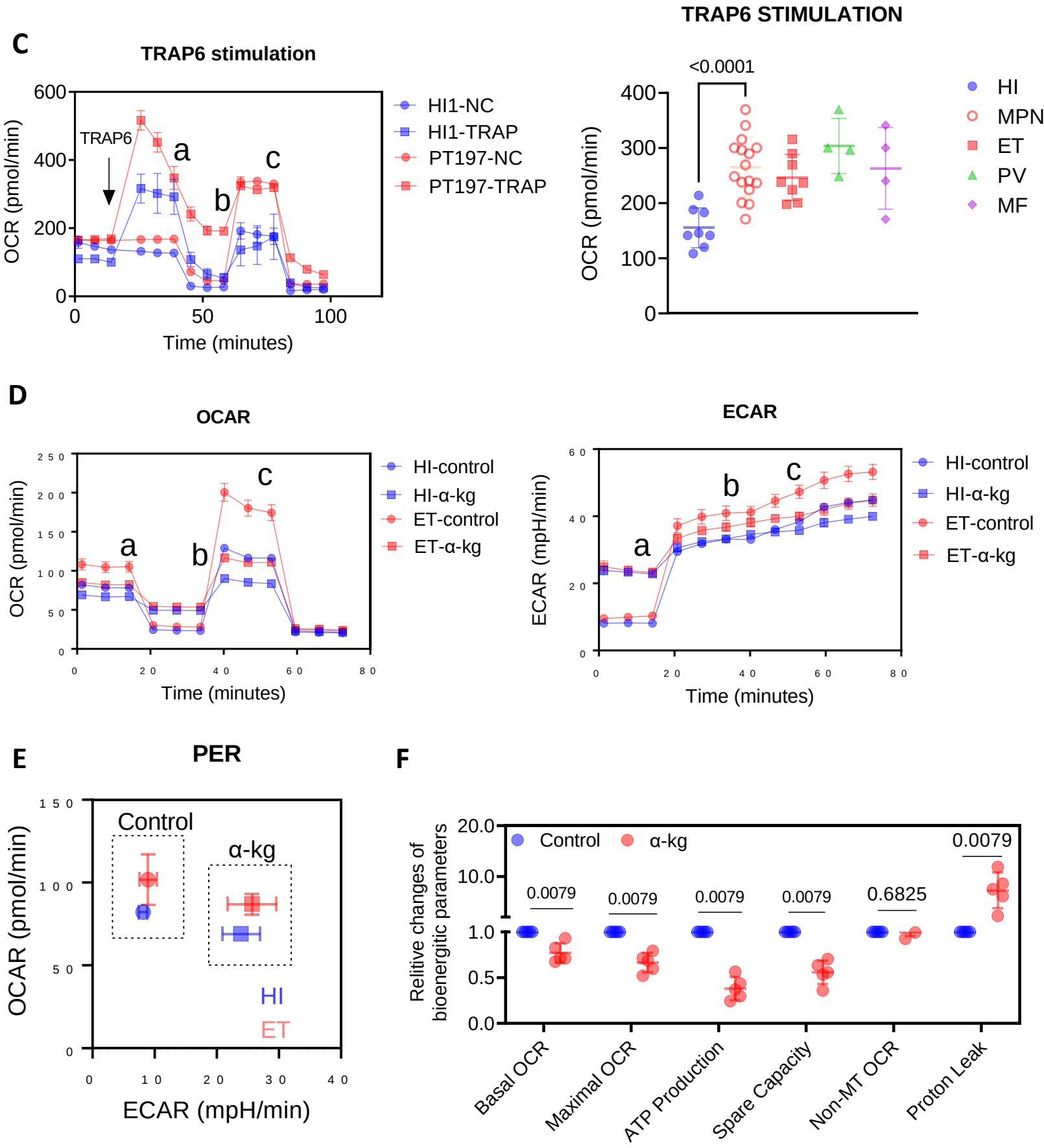
C
TRAP6 stimulation
OCR (pmol/min)
Time (minutes)
TRAP6
a
b
c
HI1-NC
HI1-TRAP
PT197-NC
PT197-TRAP
TRAP6 STIMULATION
<0.0001
OCR (pmol/min)
HI
MPN
ET
PV
MF
D
OCAR
OCR (pmol/min)
Time (minutes)
HI-control
HI-α-kg
ET-control
ET-α-kg
ECAR
ECAR (mpH/min)
Time (minutes)
E
PER
OCAR (pmol/min)
ECAR (mpH/min)
Control
α-kg
HI
ET
F
Relitive changes of bioenergitic parameters
Control
α-kg
0.0079
0.0079
0.0079
0.0079
0.6825
0.0079
Basal OCR
Maximal OCR
ATP Production
Spare Capacity
Non-MT OCR
Proton Leak

Figure 5

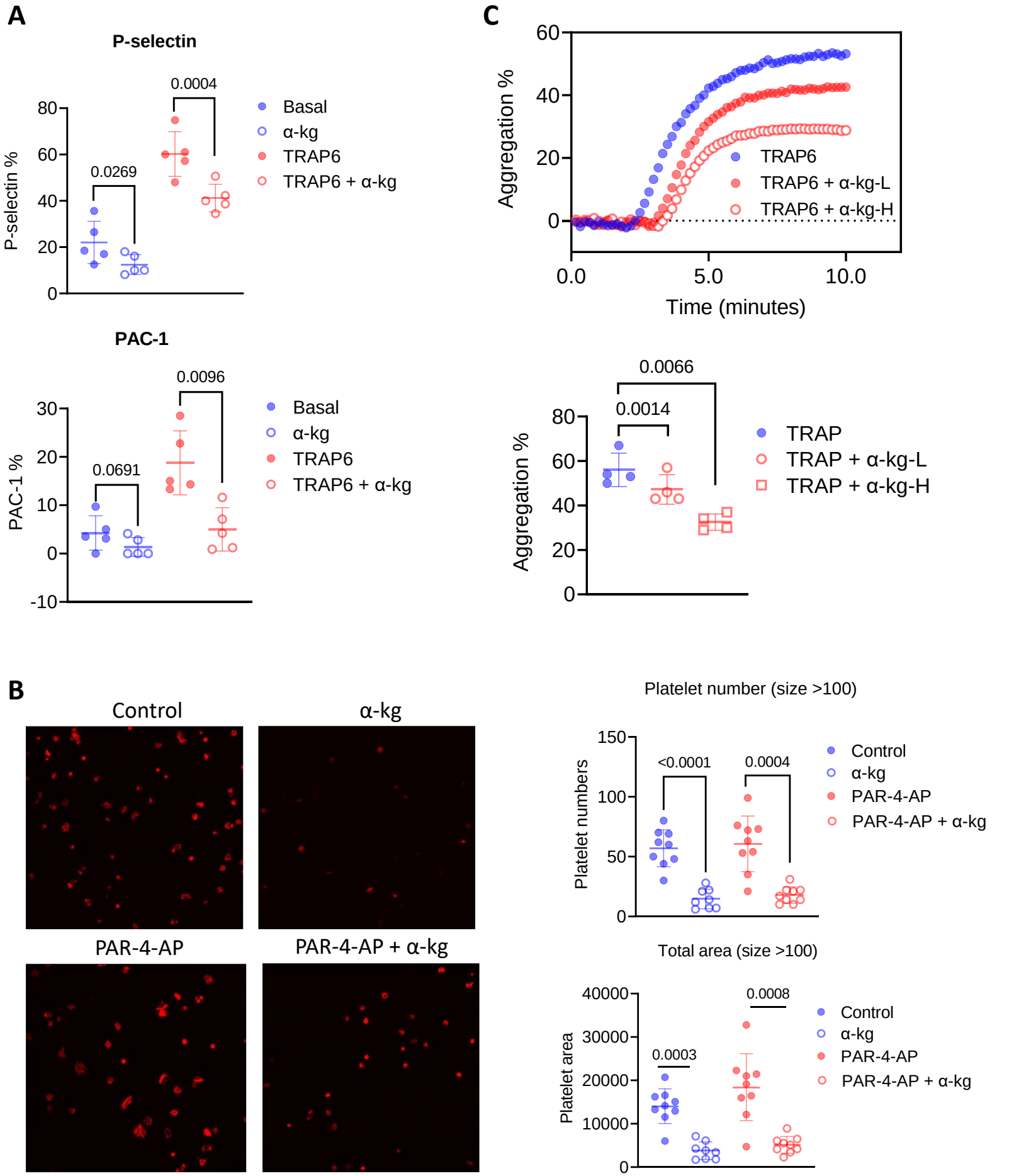
A
P-selectin
P-selectin %
0.0269
0.0004
Basal
α-kg
TRAP6
TRAP6 + α-kg
PAC-1
PAC-1 %
0.0691
0.0096
Basal
α-kg
TRAP6
TRAP6 + α-kg
C
Aggregation %
Time (minutes)
TRAP6
TRAP6 + α-kg-L
TRAP6 + α-kg-H
Aggregation %
0.0014
0.0066
TRAP
TRAP + α-kg-L
TRAP + α-kg-H
B
Control
α-kg
PAR-4-AP
PAR-4-AP + α-kg
Platelet number (size >100)
Platelet numbers
<0.0001
0.0004
Control
α-kg
PAR-4-AP
PAR-4-AP + α-kg
Total area (size >100)
Platelet area
0.0003
0.0008
Control
α-kg
PAR-4-AP
PAR-4-AP + α-kg

Figure 5

D

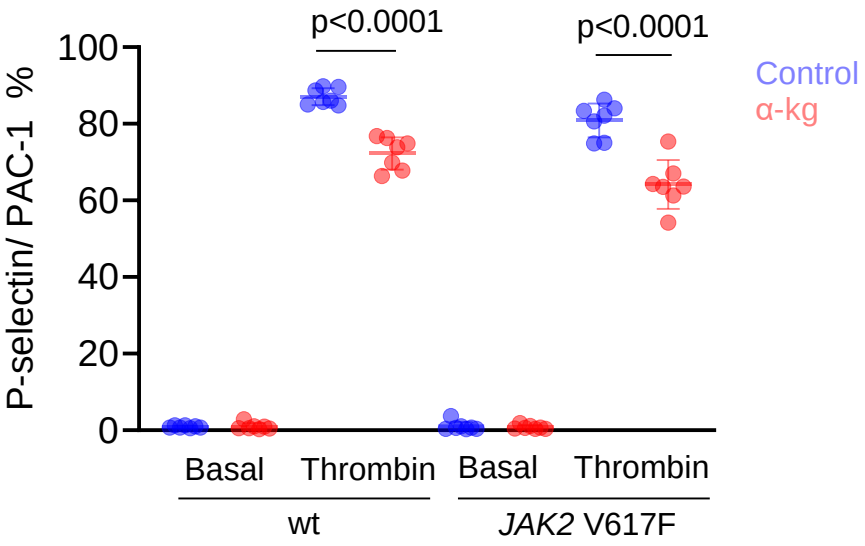

E

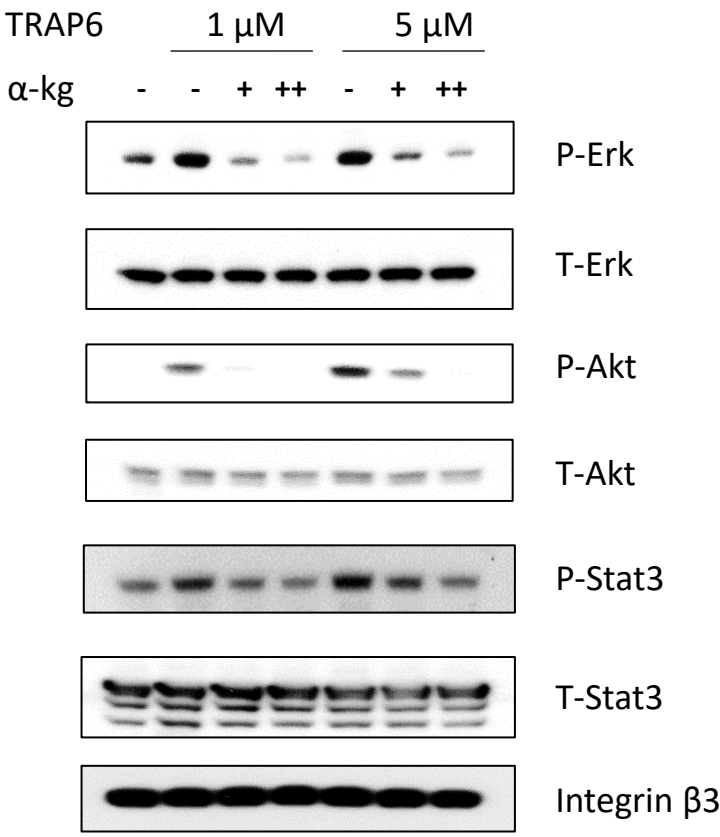

F

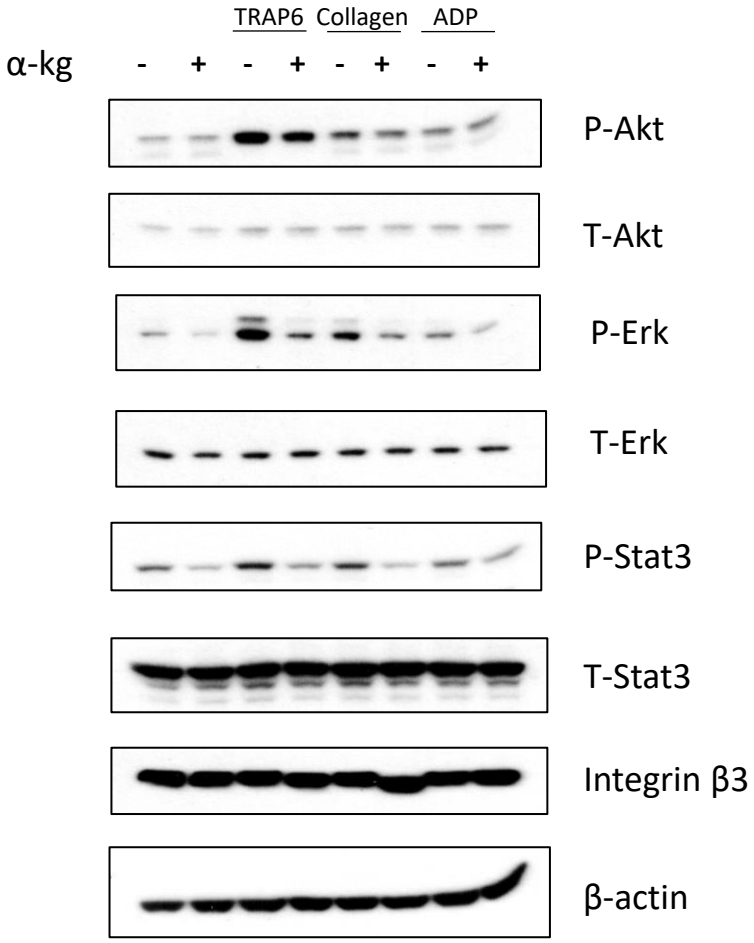

G

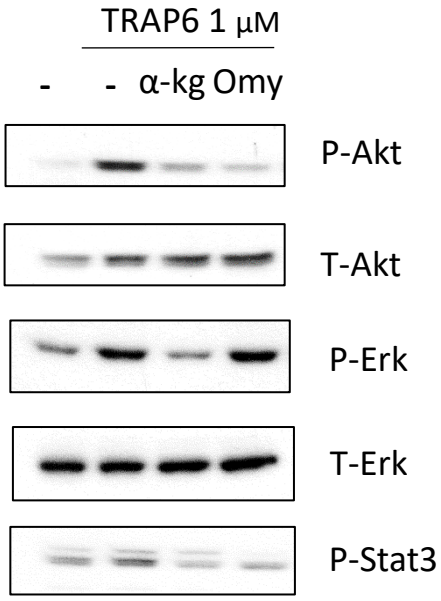

Figure 6

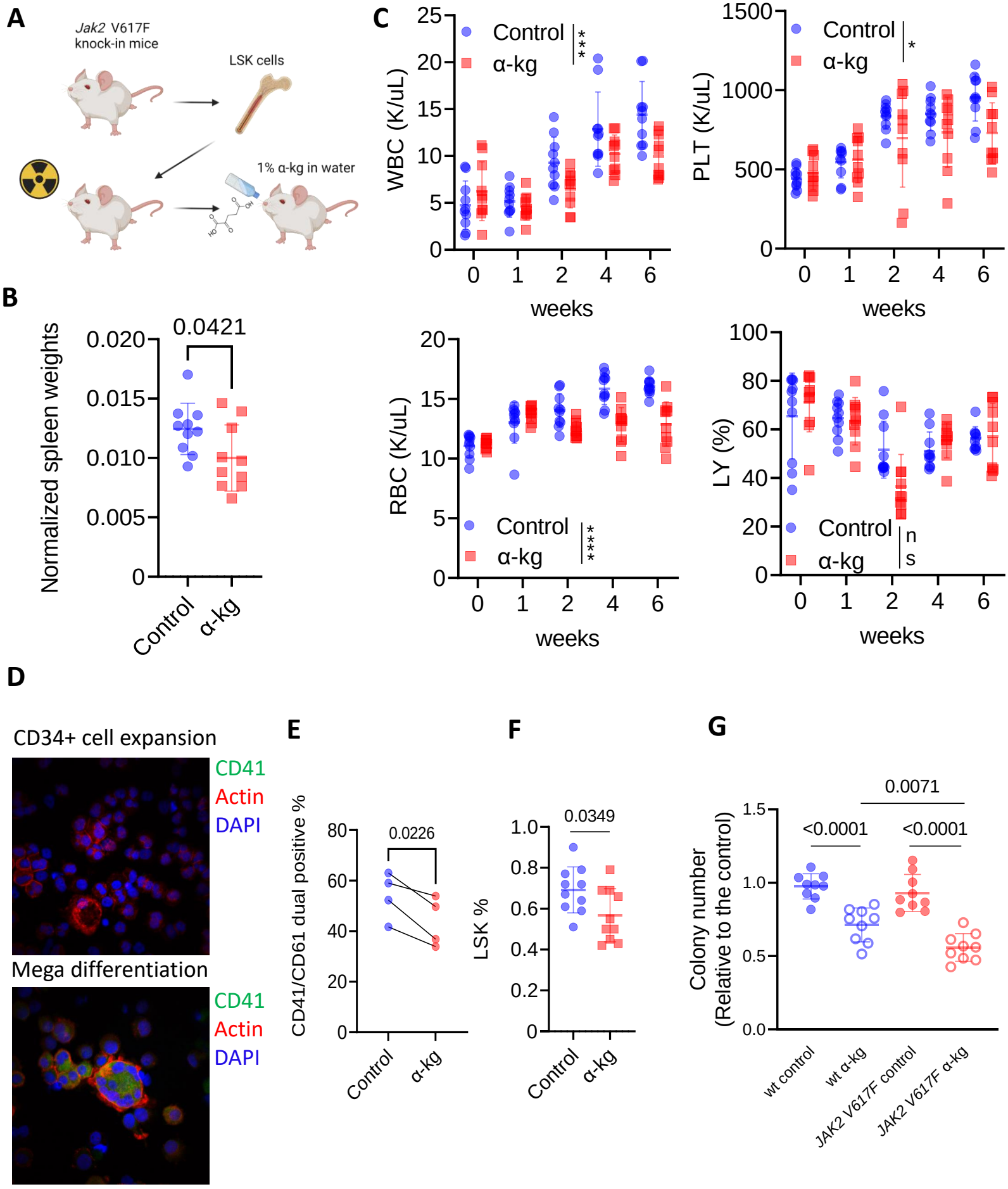
A
Jak2 V617F knock-in mice
LSK cells
1% α-kg in water
B
Normalized spleen weights
0.0421
Control
α-kg
C
WBC (K/uL)
PLT (K/uL)
RBC (K/uL)
LY (%)
Control
α-kg
weeks
D
CD34+ cell expansion
CD41
Actin
DAPI
Mega differentiation
E
CD41/CD61 dual positive %
0.0226
F
LSK %
0.0349
G
Colony number (Relative to the control)
0.0071
<0.0001
wt control
wt α-kg
JAK2 V617F control
JAK2 V617F α-kg

Figure 7

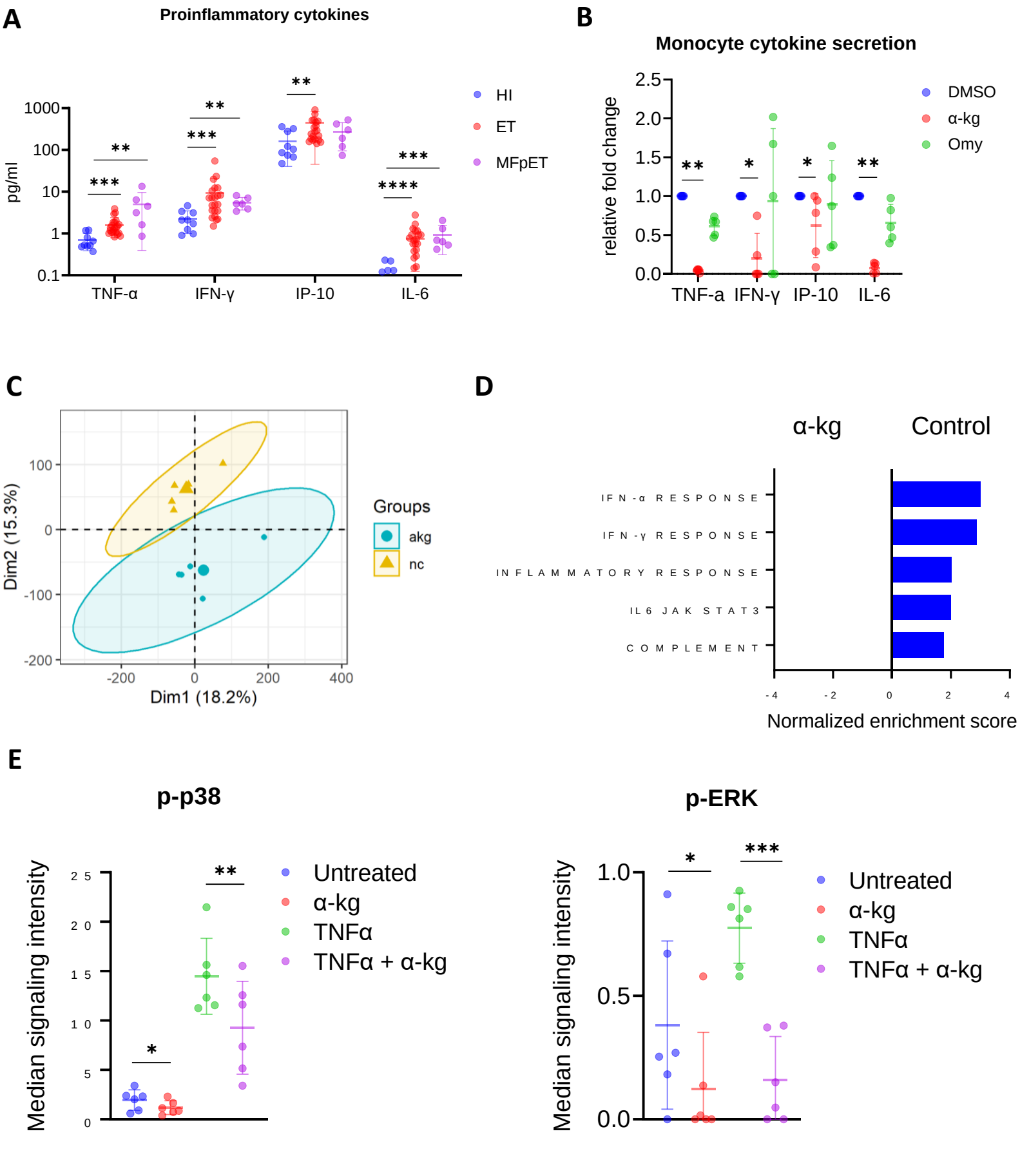
A
Proinflammatory cytokines
pg/ml
1000
100
10
1
0.1
TNF-α
IFN-γ
IP-10
IL-6
HI
ET
MFpET
B
Monocyte cytokine secretion
relative fold change
2.5
2.0
1.5
1.0
0.5
0.0
TNF-a
IFN-γ
IP-10
IL-6
DMSO
α-kg
Omy
C
Dim2 (15.3%)
Dim1 (18.2%)
Groups
akg
nc
D
α-kg
Control
IFN-α RESPONSE
IFN-γ RESPONSE
INFLAMMATORY RESPONSE
IL6 JAK STAT3
COMPLEMENT
Normalized enrichment score
E
p-p38
Median signaling intensity
Untreated
α-kg
TNFα
TNFα + α-kg
p-ERK
Median signaling intensity
Untreated
α-kg
TNFα
TNFα + α-kg

Figure S1

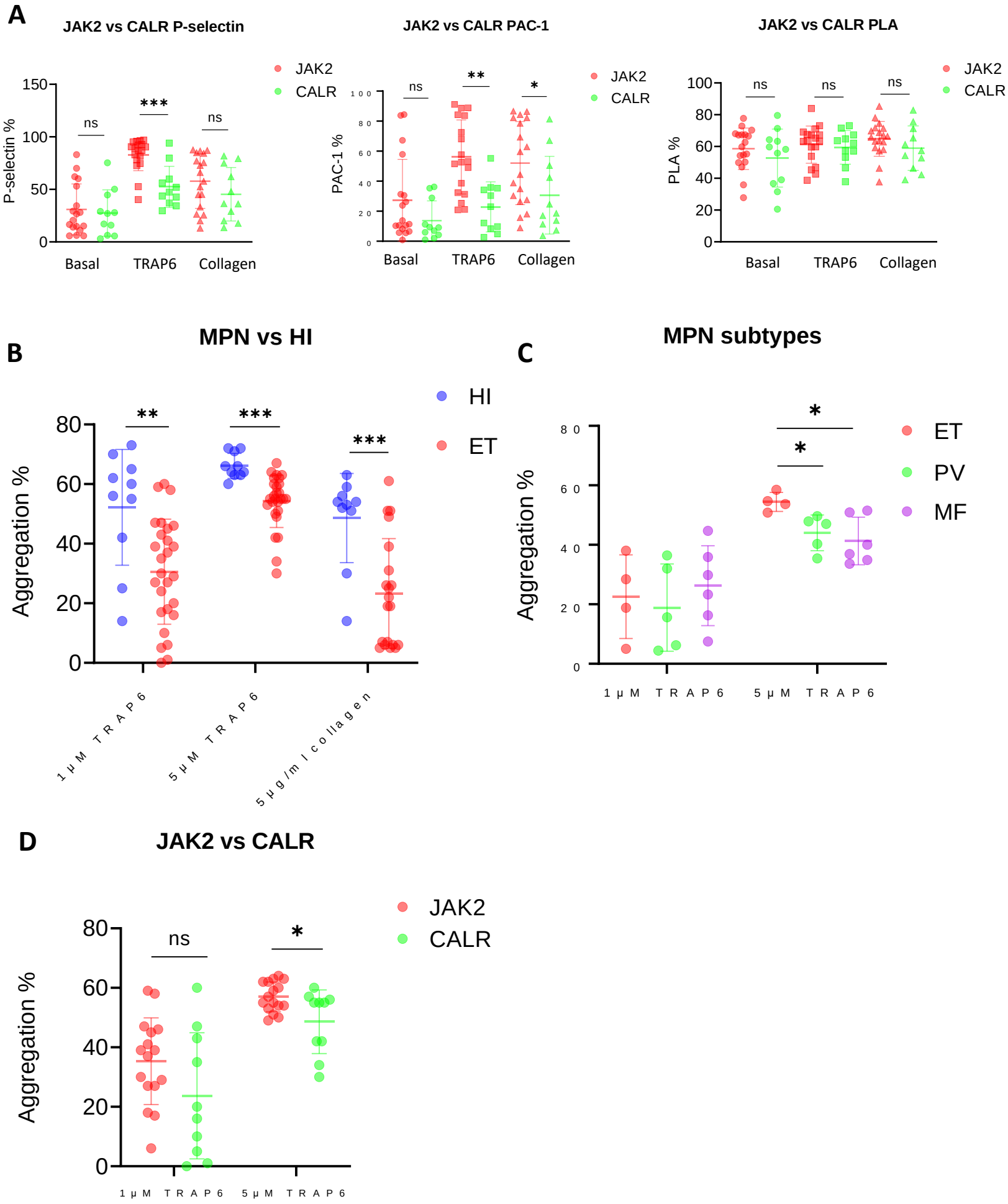
A
JAK2 vs CALR P-selectin
JAK2
CALR
P-selectin %
150
100
50
0
ns
***
ns
Basal
TRAP6
Collagen
JAK2 vs CALR PAC-1
PAC-1 %
ns
**
*
JAK2 vs CALR PLA
PLA %
ns
ns
ns
B
MPN vs HI
HI
ET
Aggregation %
80
60
40
20
0
**
***
***
1 µM TRAP6
5 µM TRAP6
5 µg/ml collagen
C
MPN subtypes
ET
PV
MF
Aggregation %
*
*
1 µM TRAP6
5 µM TRAP6
D
JAK2 vs CALR
JAK2
CALR
Aggregation %
ns
*
1 µM TRAP6
5 µM TRAP6

Figure S2

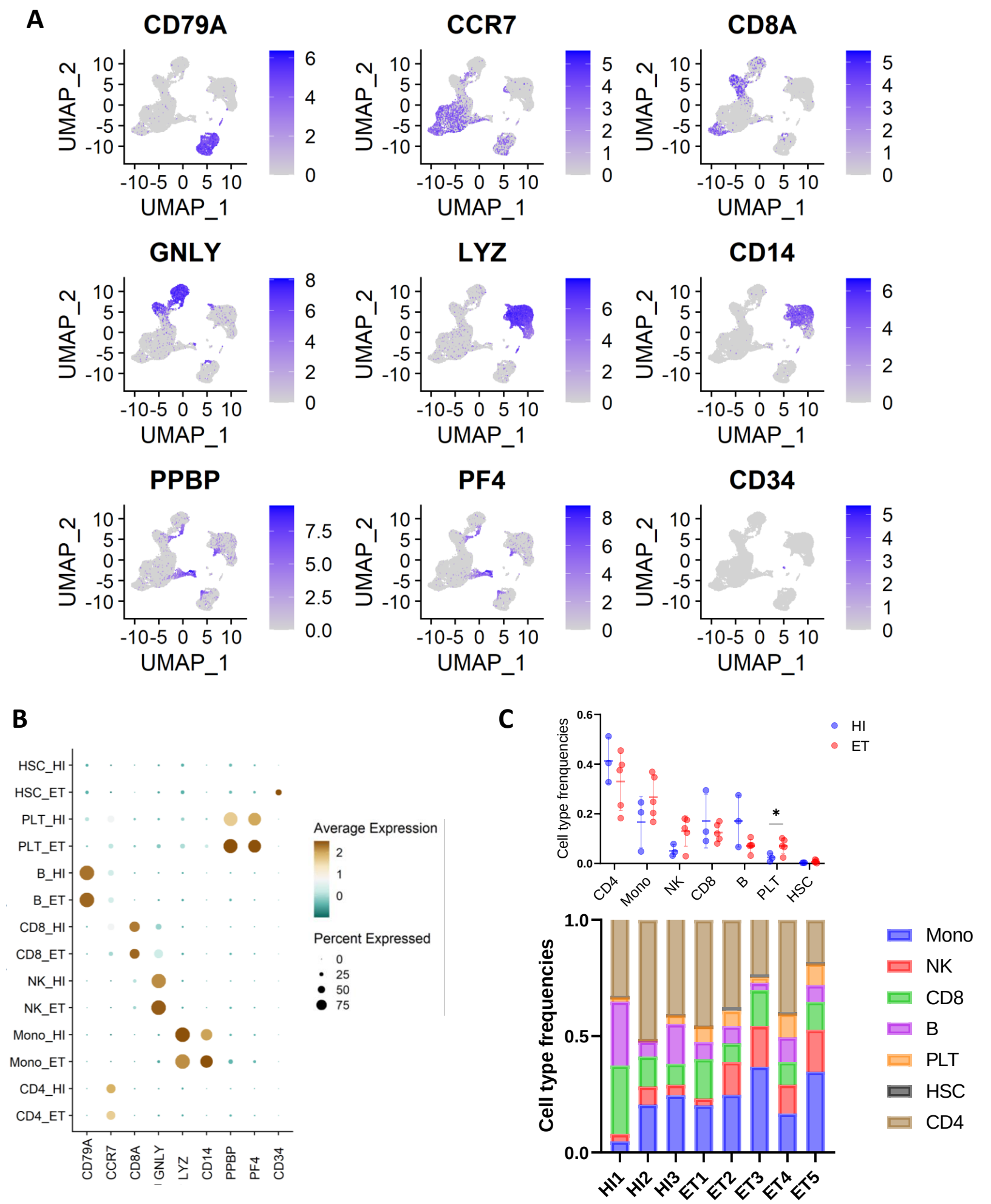
A
CD79A
CCR7
CD8A
GNLY
LYZ
CD14
PPBP
PF4
CD34
UMAP_1
UMAP_2
B
HSC_HI
HSC_ET
PLT_HI
PLT_ET
B_HI
B_ET
CD8_HI
CD8_ET
NK_HI
NK_ET
Mono_HI
Mono_ET
CD4_HI
CD4_ET
Average Expression
Percent Expressed
C
HI
ET
Cell type frenquencies
CD4
Mono
NK
CD8
B
PLT
HSC
Cell type frequencies
HI1
HI2
HI3
ET1
ET2
ET3
ET4
ET5
Mono
NK
CD8
B
PLT
HSC
CD4

Figure S2

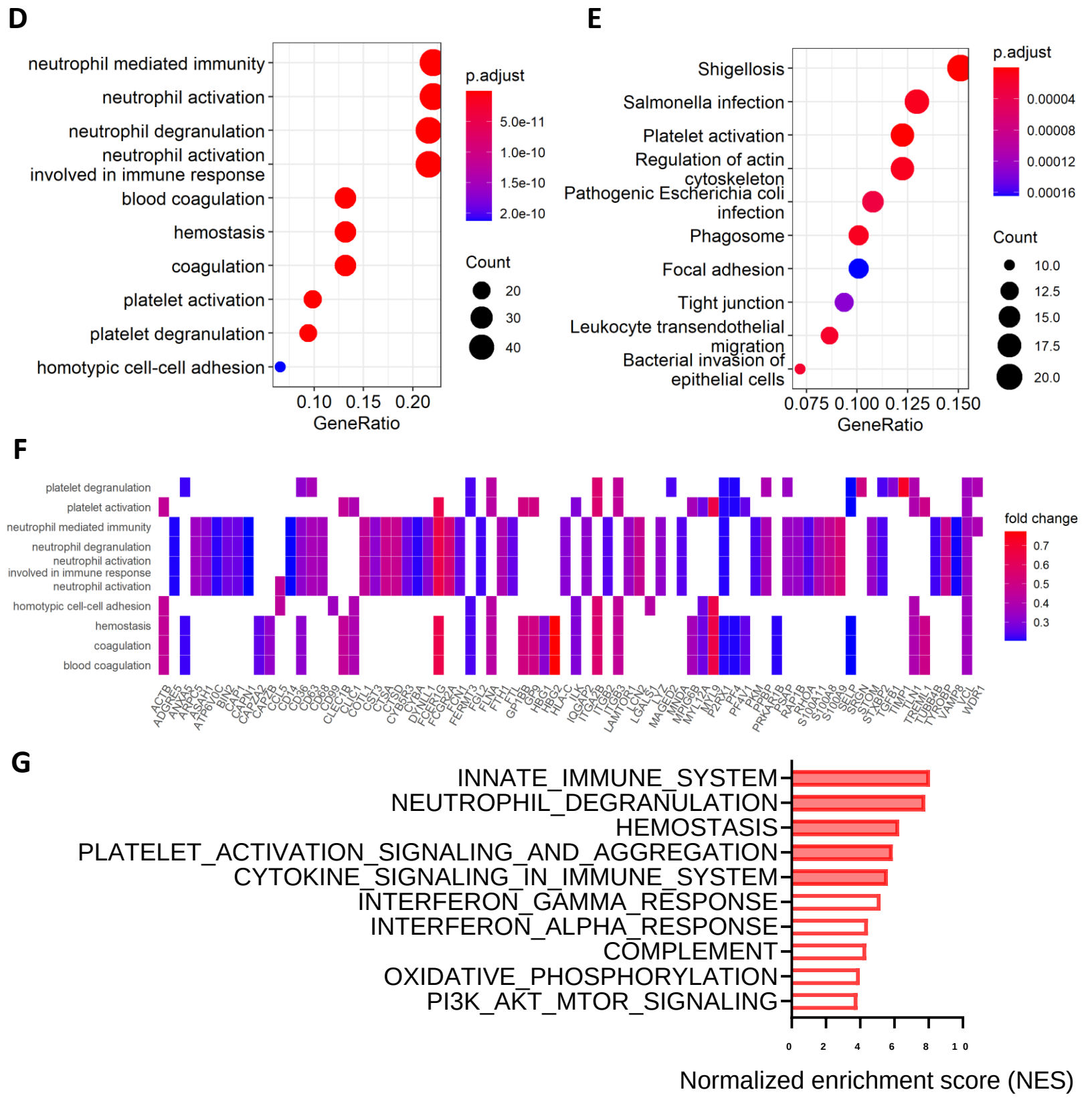
D
neutrophil mediated immunity
neutrophil activation
neutrophil degranulation
neutrophil activation involved in immune response
blood coagulation
hemostasis
coagulation
platelet activation
platelet degranulation
homotypic cell-cell adhesion
0.10 0.15 0.20
GeneRatio
p.adjust
5.0e-11
1.0e-10
1.5e-10
2.0e-10
Count
20
30
40
E
Shigellosis
Salmonella infection
Platelet activation
Regulation of actin cytoskeleton
Pathogenic Escherichia coli infection
Phagosome
Focal adhesion
Tight junction
Leukocyte transendothelial migration
Bacterial invasion of epithelial cells
0.075 0.100 0.125 0.150
GeneRatio
p.adjust
0.00004
0.00008
0.00012
0.00016
Count
10.0
12.5
15.0
17.5
20.0
F
platelet degranulation
platelet activation
neutrophil mediated immunity
neutrophil degranulation
neutrophil activation involved in immune response
neutrophil activation
homotypic cell-cell adhesion
hemostasis
coagulation
blood coagulation
ACTB ADGRE5 ANXA5 ARPC5 ASAH1 ATP6V0C BIN2 CAPN1 CAPZA1 CAPZA2 CAPZB CCL5 CD14 CD36 CD63 CD68 CD99 CLEC1B CLIC1 COTL1 CST3 CTSA CTSD CYBSR3 CYNIP DYNLL1 FCER1G FCGR2A FCN1 FERMT3 FGL2 FLNA FTH1 FTL GP1BB GP9 HBG1 HBG2 HLA-C ILK IQGAP2 ITGA2B ITGB2 ITGB3 LAMTOR1 LCN2 LGALS1 LYZ MAGED2 MNDA MPG6B MYL12A MYL9 P2RX1 PF4 PF4V1 PKM PPBP PRKAR1B RSAP RAP1B RHOA S100A11 S100A8 S100A9 SELP SRGN STOM SYBP2 TGFB1 TIMP1 TREML1 TUBB4B TYROBP VAMP8 VCL WDR1
fold change
0.7
0.6
0.5
0.4
0.3
G
INNATE_IMMUNE_SYSTEM
NEUTROPHIL_DEGRANULATION
HEMOSTASIS
PLATELET_ACTIVATION_SIGNALING_AND_AGGREGATION
CYTOKINE_SIGNALING_IN_IMMUNE_SYSTEM
INTERFERON_GAMMA_RESPONSE
INTERFERON_ALPHA_RESPONSE
COMPLEMENT
OXIDATIVE_PHOSPHORYLATION
PI3K_AKT_MTOR_SIGNALING
0 2 4 6 8 10
Normalized enrichment score (NES)
H
ES
0.4
0.3
0.2
0.1
0
0 5,000 10,000
Rank
I
ES
0.3
0.2
0.1
0
0 5,000 10,000
Rank
J
ES
0.3
0.2
0.1
0
0 5,000 10,000
Rank

Figure S3

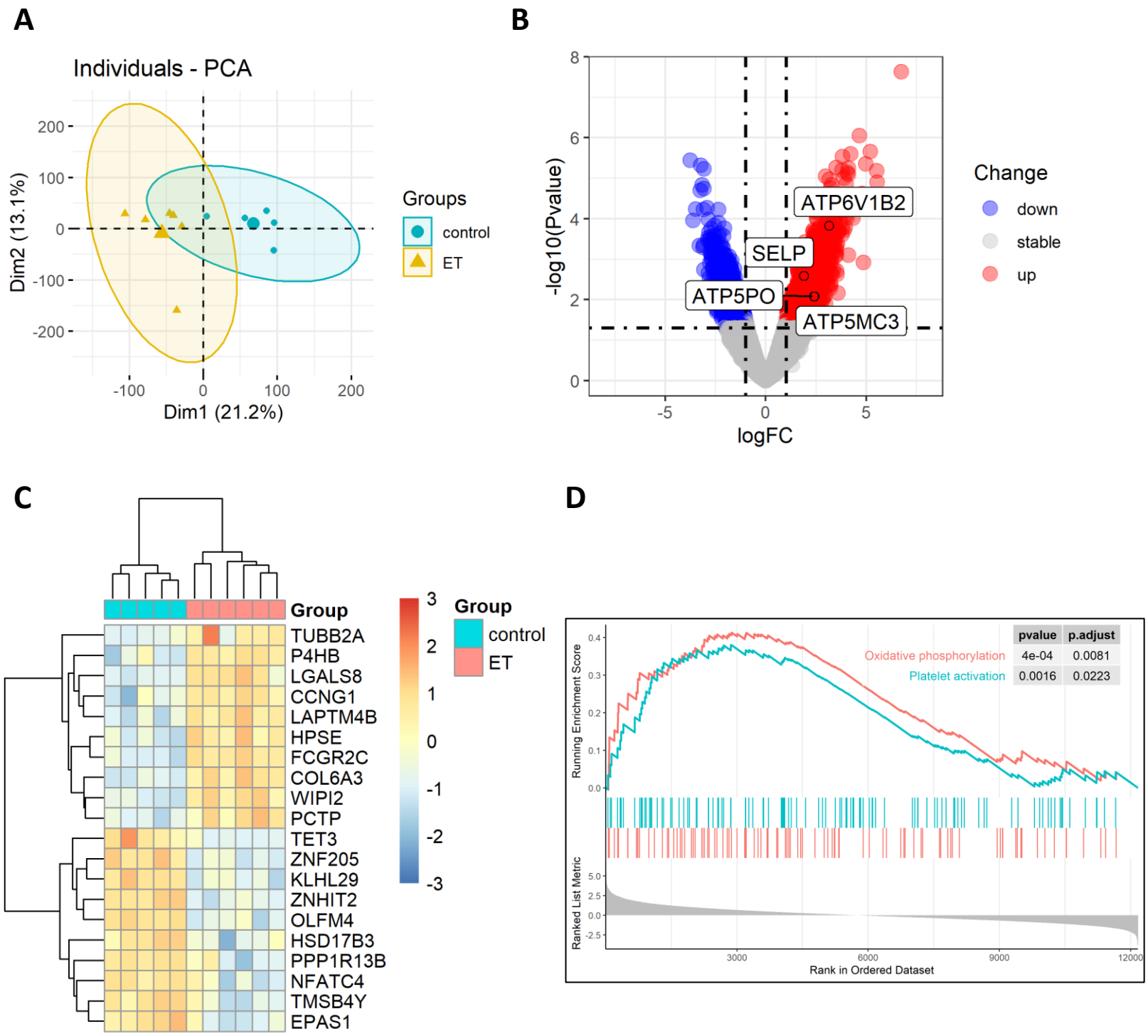

Gnatenko et al, Thromb Haemost, 2005

Figure S4

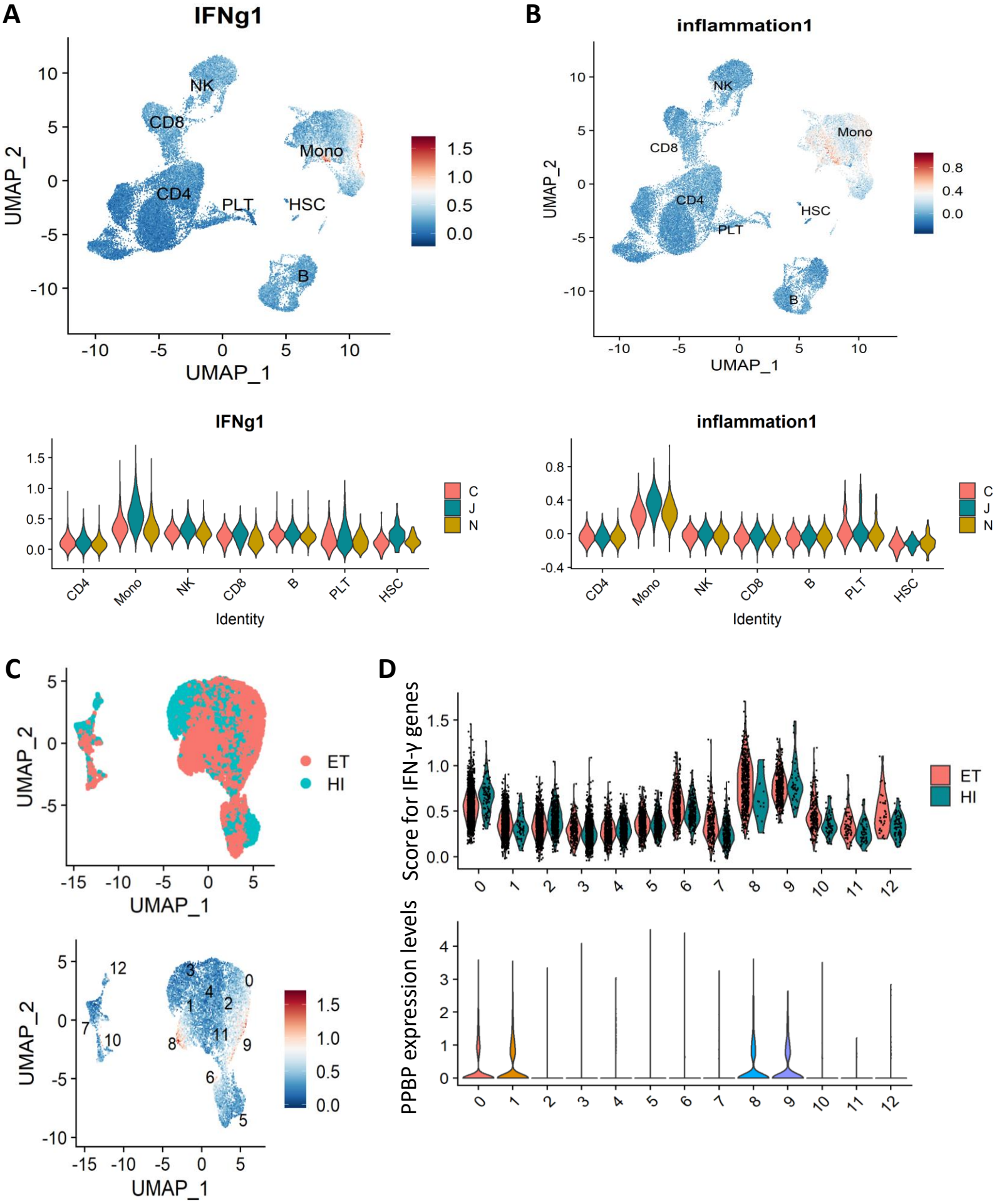
A
IFNg1
NK
CD8
Mono
CD4
PLT
HSC
B
UMAP_2
UMAP_1
B
inflammation1
IFNg1
inflammation1
C
J
N
CD4
Mono
NK
CD8
B
PLT
HSC
Identity
C
ET
HI
D
Score for IFN-γ genes
PPBP expression levels

Figure S5

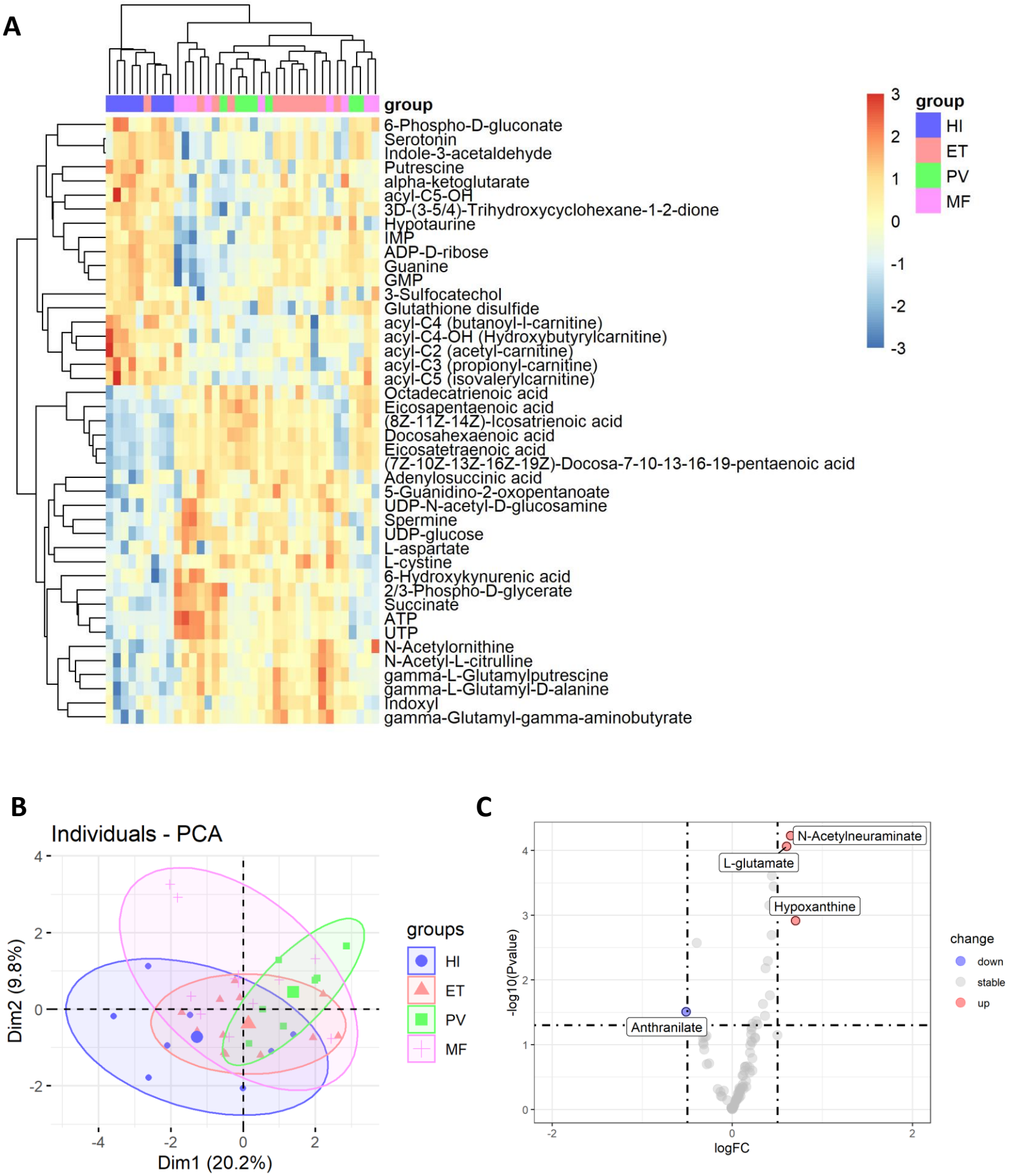
A
group
6-Phospho-D-gluconate
Serotonin
Indole-3-acetaldehyde
Putrescine
alpha-ketoglutarate
acyl-C5-OH
3D-(3-5/4)-Trihydroxycyclohexane-1-2-dione
Hypotaurine
IMP
ADP-D-ribose
Guanine
GMP
3-Sulfocatechol
Glutathione disulfide
acyl-C4 (butanoyl-l-carnitine)
acyl-C4-OH (Hydroxybutyrylcarnitine)
acyl-C2 (acetyl-carnitine)
acyl-C3 (propionyl-carnitine)
acyl-C5 (isovalerylcarnitine)
Octadecatrienoic acid
Eicosapentaenoic acid
(8Z-11Z-14Z)-Icosatrienoic acid
Docosahexaenoic acid
Eicosatetraenoic acid
(7Z-10Z-13Z-16Z-19Z)-Docosa-7-10-13-16-19-pentaenoic acid
Adenylosuccinic acid
5-Guanidino-2-oxopentanoate
UDP-N-acetyl-D-glucosamine
Spermine
UDP-glucose
L-aspartate
L-cystine
6-Hydroxykynurenic acid
2/3-Phospho-D-glycerate
Succinate
ATP
UTP
N-Acetylornithine
N-Acetyl-L-citrulline
gamma-L-Glutamylputrescine
gamma-L-Glutamyl-D-alanine
Indoxyl
gamma-Glutamyl-gamma-aminobutyrate
3
2
1
0
-1
-2
-3
group
HI
ET
PV
MF
B
Individuals - PCA
Dim2 (9.8%)
Dim1 (20.2%)
4
2
0
-2
-4
-2
0
2
groups
HI
ET
PV
MF
C
N-Acetylneuraminate
L-glutamate
Hypoxanthine
Anthranilate
-log10(Pvalue)
logFC
change
down
stable
up

Figure S6

A

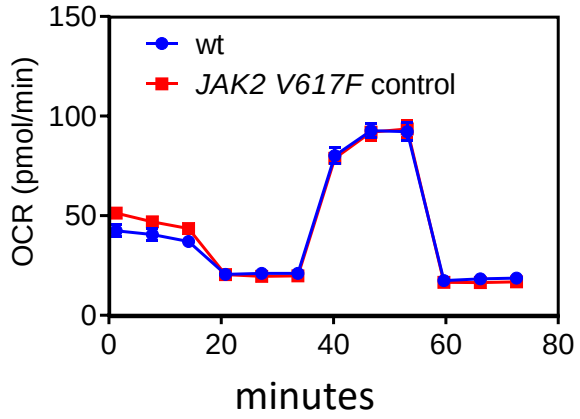

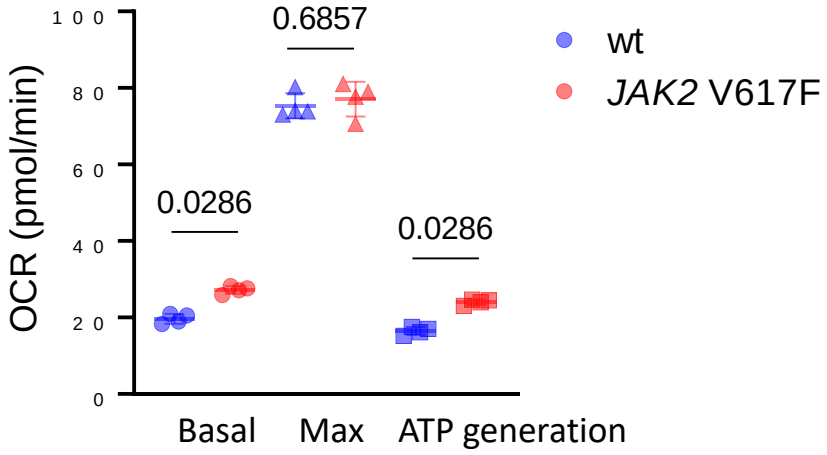

B

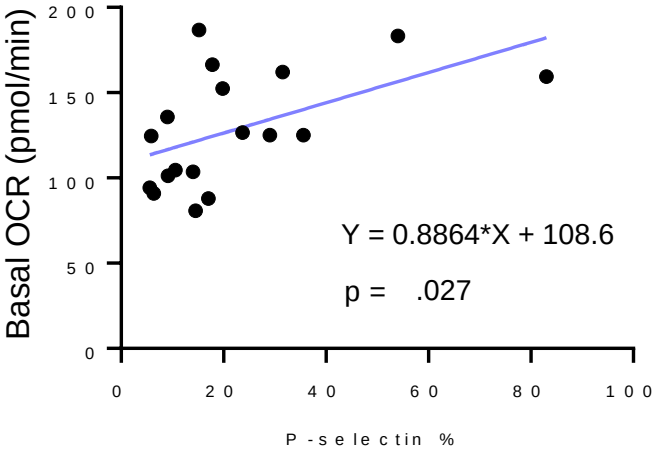

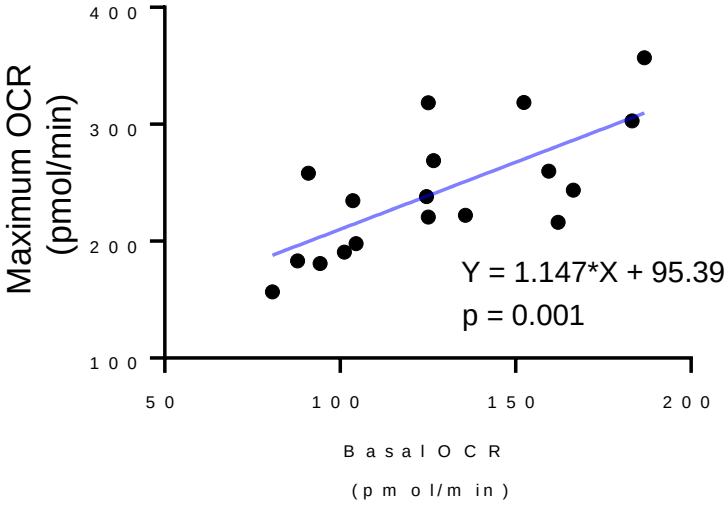

C

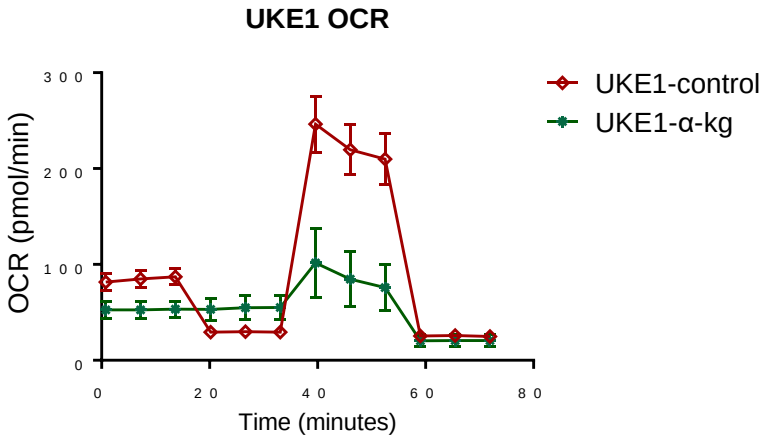

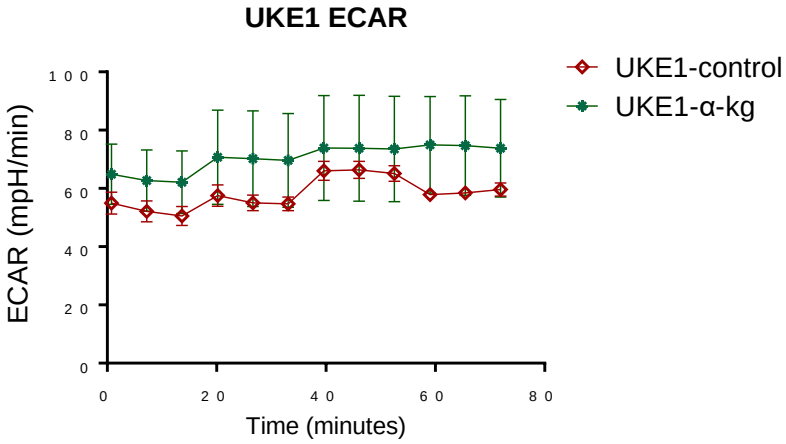

Figure S7

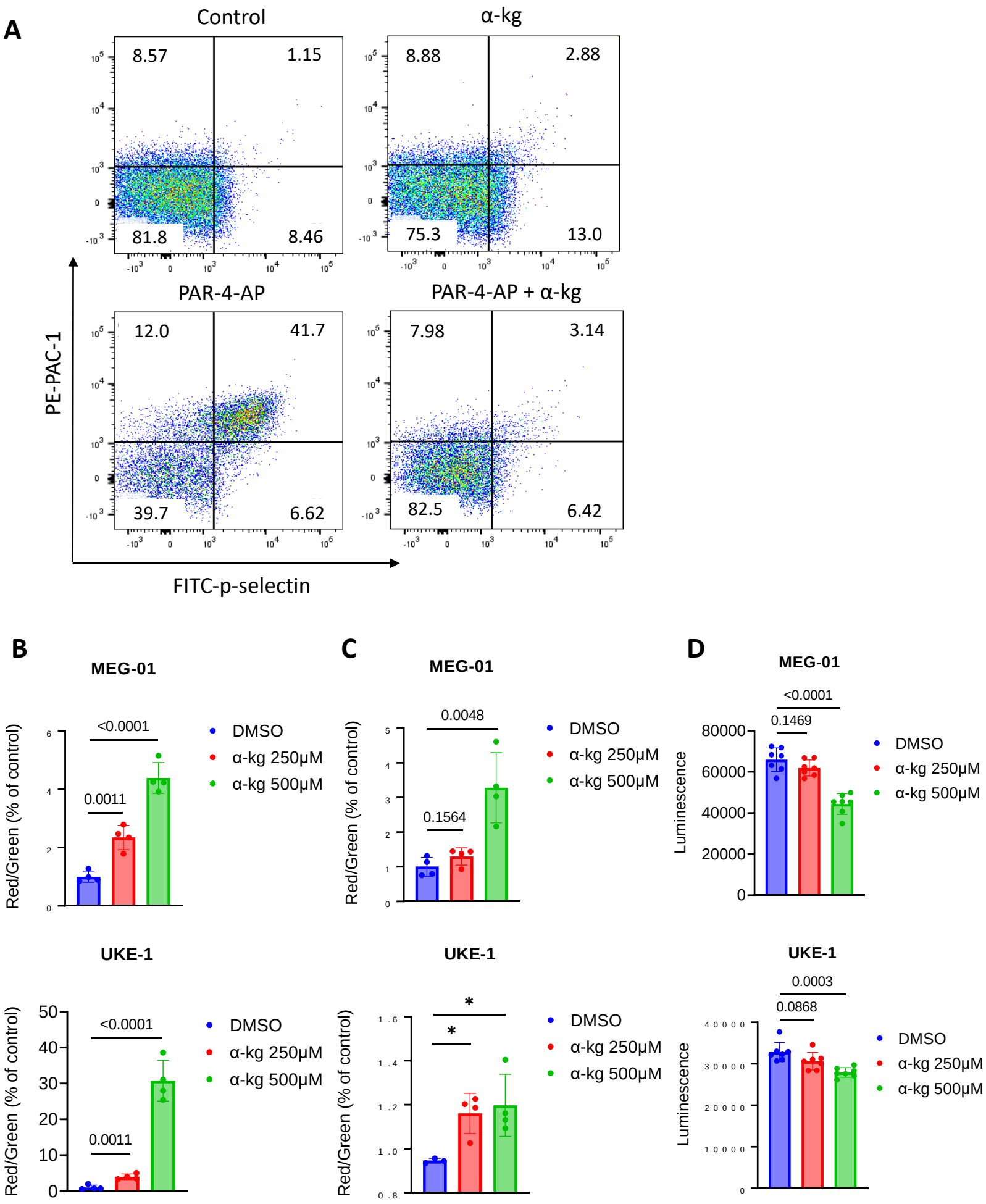
A
Control
8.57
1.15
81.8
8.46
α-kg
8.88
2.88
75.3
13.0
PAR-4-AP
12.0
41.7
39.7
6.62
PAR-4-AP + α-kg
7.98
3.14
82.5
6.42
PE-PAC-1
FITC-p-selectin
B
MEG-01
<0.0001
0.0011
Red/Green (% of control)
DMSO
α-kg 250μM
α-kg 500μM
UKE-1
<0.0001
0.0011
C
MEG-01
0.0048
0.1564
UKE-1
*
*
D
MEG-01
<0.0001
0.1469
Luminescence
UKE-1
0.0003
0.0868

Figure S8

A

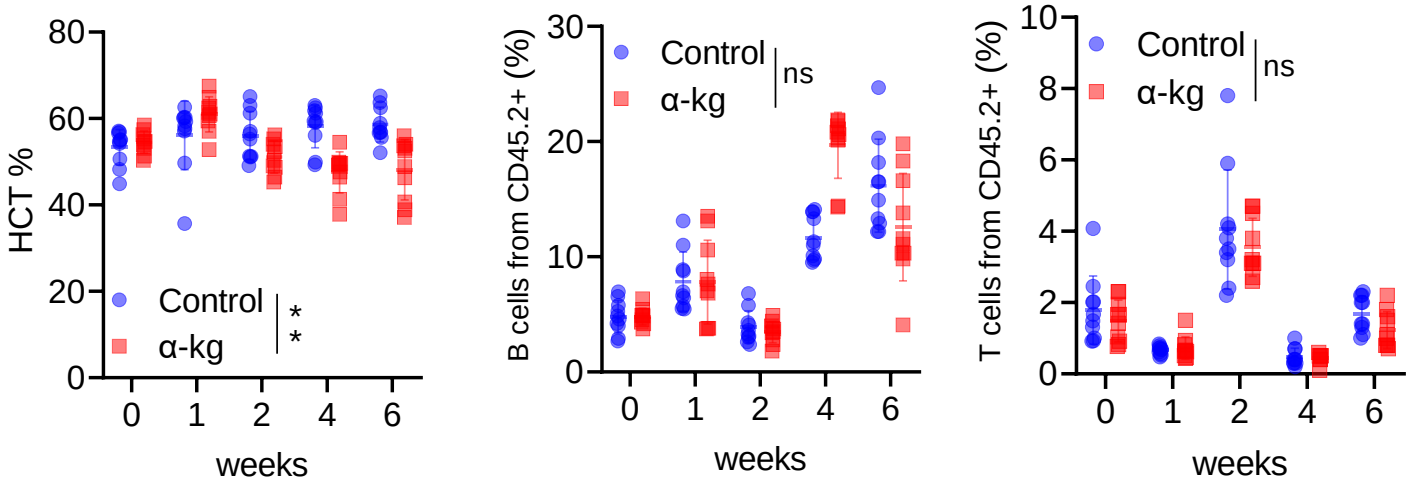

B

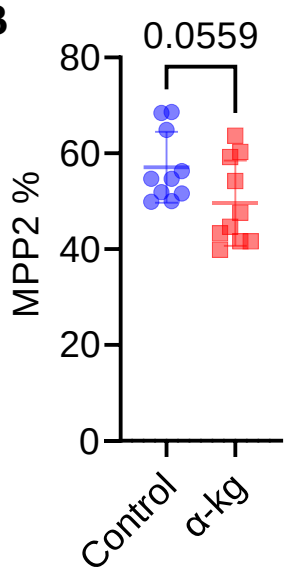

C

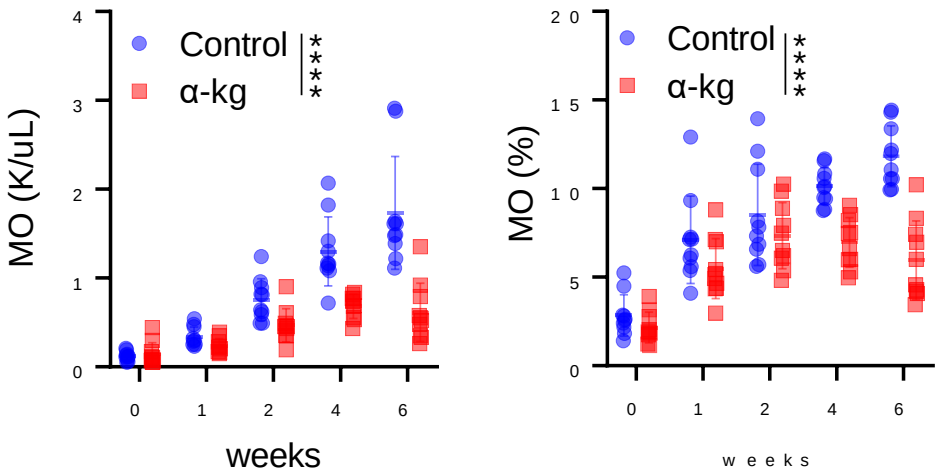

D

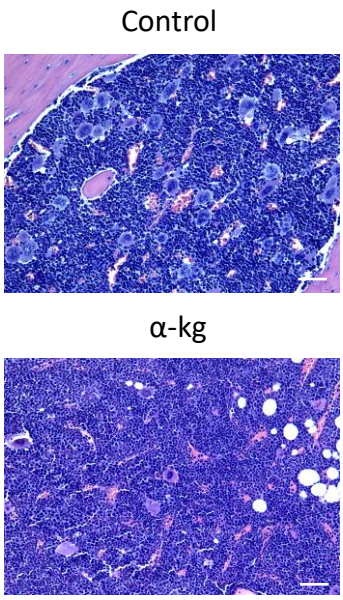

E

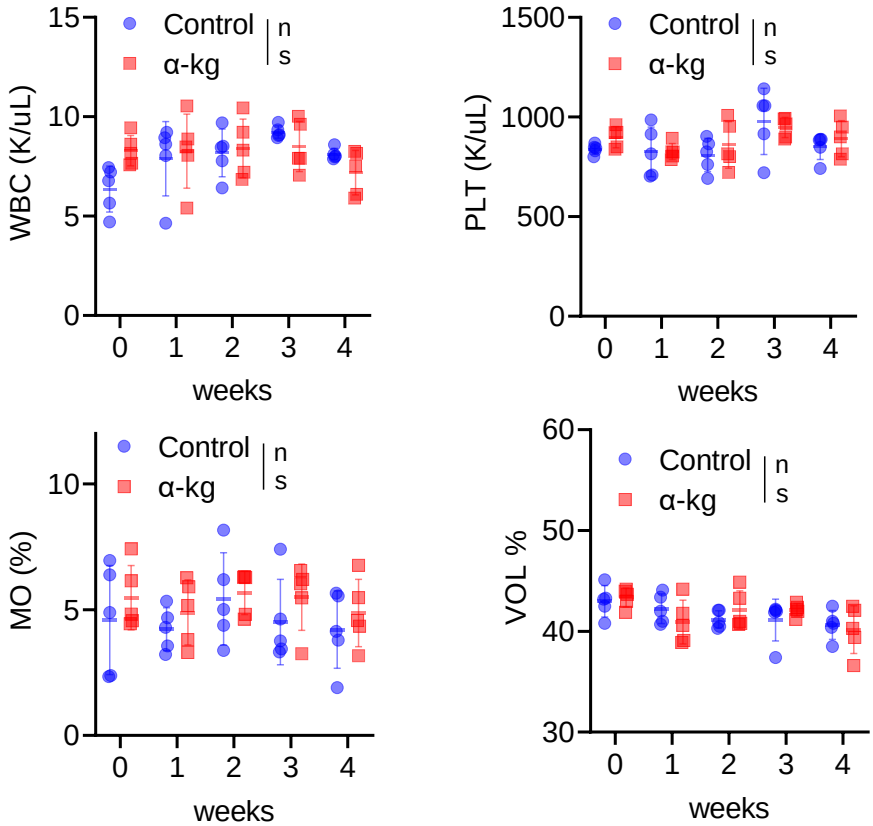

Figure S8

F

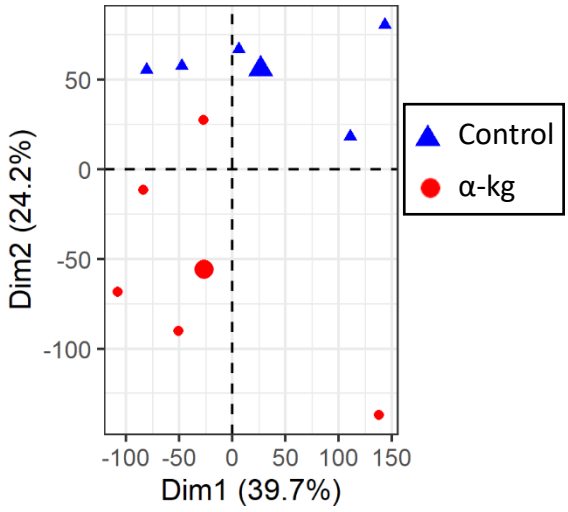

G

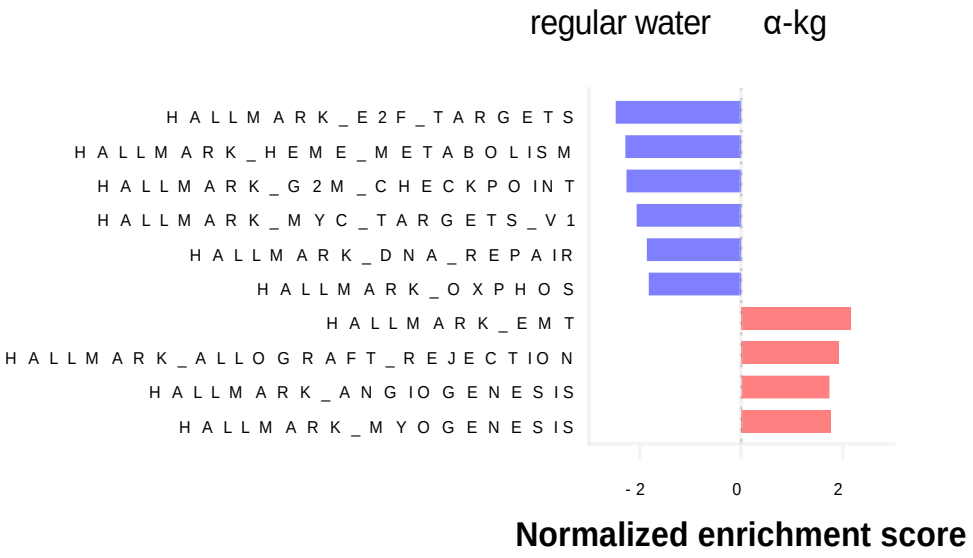

H

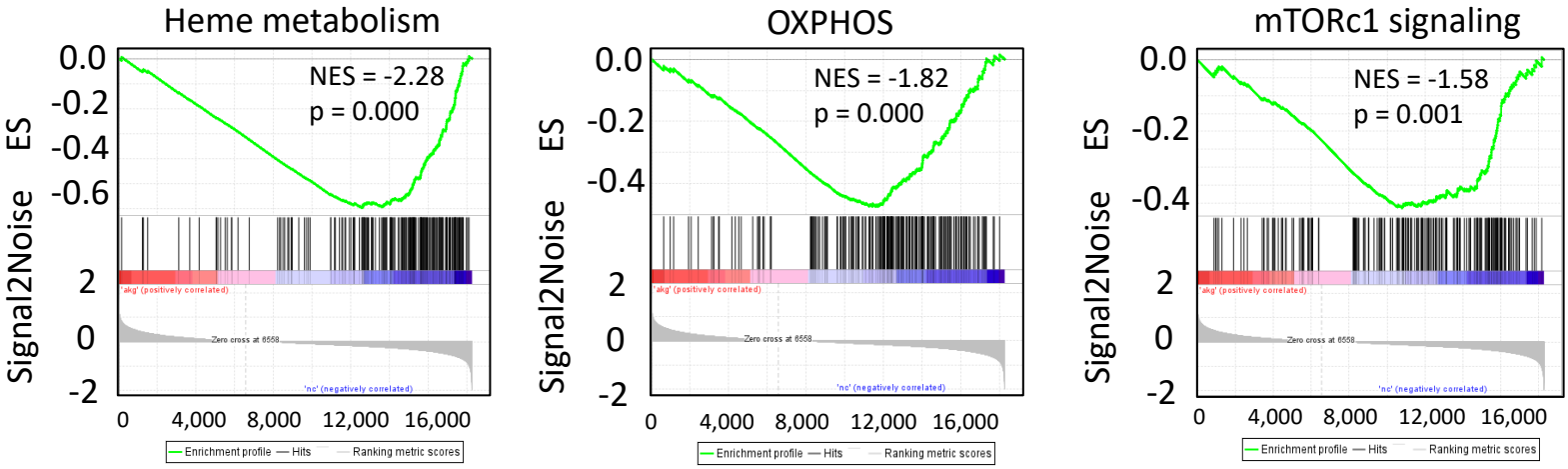

I

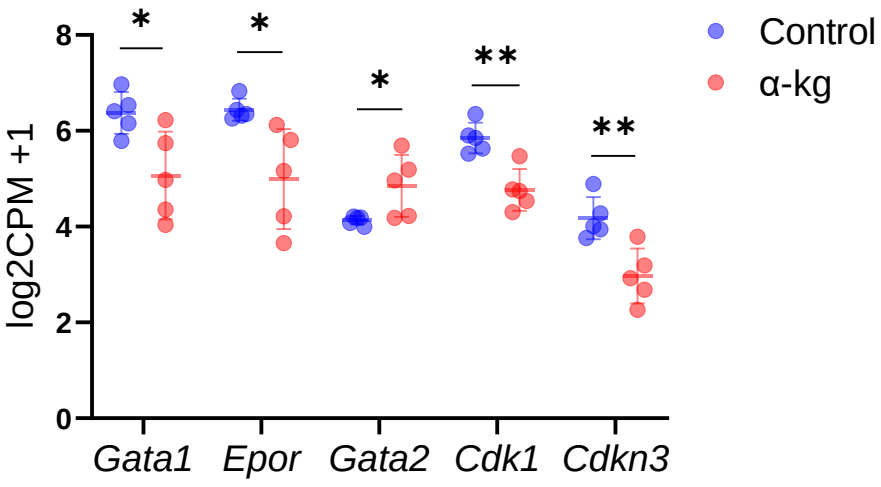

Figure S8

J

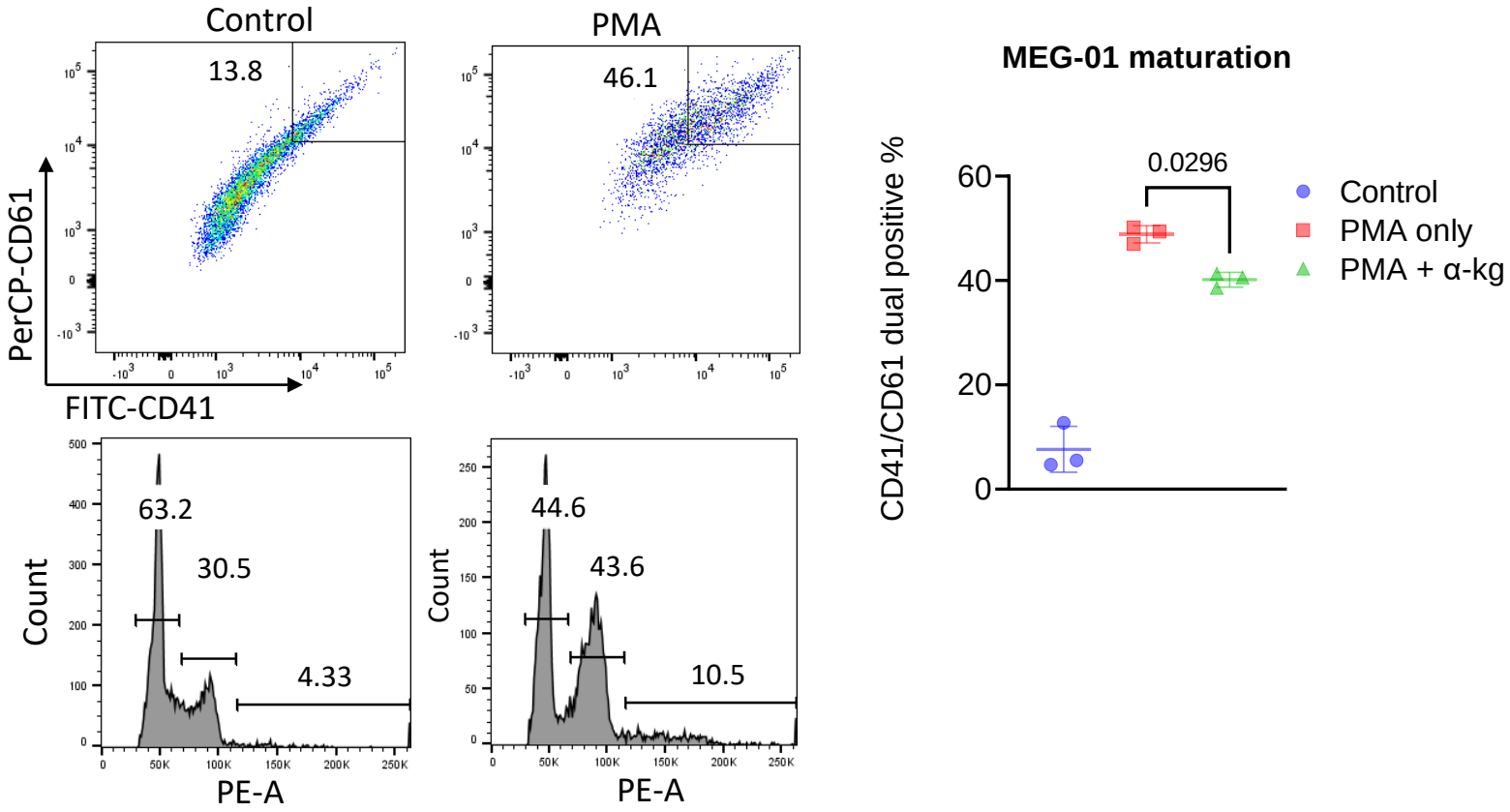
Control
PMA
13.8
46.1
PerCP-CD61
FITC-CD41
63.2
30.5
4.33
44.6
43.6
10.5
Count
PE-A
MEG-01 maturation
CD41/CD61 dual positive %
0.0296
Control
PMA only
PMA + α-kg